



21 **Key points**

22 Surface-subsurface flow coupling

23

24 **Abstract**

25 Commonly, the dual node approach for coupling surface-subsurface flow is conceptualized as a
26 hydraulic separation of the surface and the subsurface by a distinct interface with a given thickness.
27 Since such an interface is not supported by field observations, it has been argued that the dual node
28 depends on a non-physical parameter in the form an ill-defined interface thickness. As such, the
29 alternative common node approach is considered to be a more general and a more elegant approach
30 since it is based on the physical principle of head continuity along the surface-subsurface interface.
31 In this study, however, it is argued that if properly implemented, then the dual node approach is
32 actually the more general, the more elegant as well as the more accurate approach. This insight is
33 obtained by considering that the topmost subsurface nodal values represent the mean values within
34 discrete control volumes and by deriving the dual node approach from equations that govern
35 infiltration and infiltrability. It is shown that the dual node approach should be conceptualized as
36 a simple one-sided first-order finite-difference to approximate the vertical subsurface hydraulic
37 gradient at the land surface and that there is no need to assume a hydraulic separation between the
38 two flow domains by a distinct interface. Whereas a consistent properly implemented dual node
39 approach is in agreement with the physical principle of head continuity at the land surface, it is
40 shown that the common node approach is not. Studies that have compared the two coupling
41 approaches have been based on improperly implemented dual node approaches. As such, this study
42 presents a re-evaluation of how the common node compares to the dual node approach. Cell-
43 centered as well as vertex-centered schemes are considered.



44 1 Introduction

45 There exists a variety of hydrogeological problems, such as the hydrologic response of hill slopes
46 and river catchments, which requires an integrated analysis of surface and subsurface flows. This
47 has led to the development of physically-based, distributed parameter models for simulating
48 coupled surface-subsurface flows. Well-known examples of such models include MODHMS
49 [Panday and Huyakorn, 2004], InHM [Ebel *et al.*, 2009], HydroGeoSphere [Therrien *et al.*, 2010],
50 CATHY [Weill *et al.*, 2011], WASH123D [Yeh *et al.*, 2011], ParFlow [Kollet and Maxwell, 2006]
51 and OpenGeoSys [Kolditz and Shao, 2010]. Typically, subsurface flow is governed by the
52 Richards' equation whereas surface flow is either governed by the kinematic wave or the diffusive
53 wave equation.

54 The coupling between subsurface and surface flow may be either based on the common
55 node approach [Kollet and Maxwell, 2006] or on the dual node approach [Ebel *et al.*, 2009; Panday
56 and Huyakorn, 2004; VanderKwaak, 1999]. In the common node approach coupling is formulated
57 by a continuity in head between surface and subsurface nodes. The dual node approach is based
58 on formulating an exchange flux between the surface and subsurface nodes. Typically, the dual
59 node approach is conceptualized as a hydraulic separation of the surface and the subsurface by a
60 saturated interface with a given thickness [Liggett *et al.*, 2012]. The thickness of this interface
61 defines a coupling length between the dual nodes to formulate the discrete exchange flux between
62 the dual nodes.

63 It has been argued that the coupling length is a non-physical model parameter, because
64 there is often no evidence to support the existence of a distinct interface between the two flow
65 domains [Kollet and Maxwell, 2006]. As such it appears that the common node approach is a more
66 general coupling approach [Kollet and Maxwell, 2006]. Considering that smaller coupling lengths



67 tend to improve the accuracy of the dual node approach [Ebel *et al.*, 2009; Liggett *et al.*, 2012;
68 Liggett *et al.*, 2013], it also seems that the common node approach is generally more accurate.
69 Namely, in the limit as the coupling length goes to zero, the dual node approach mimics the
70 common node approach [Ebel *et al.*, 2009]. It has been illustrated that both the dual node approach
71 as well as the common node approach are sensitive to the vertical discretization near the surface
72 [Liggett *et al.*, 2012; Sulis *et al.*, 2010].

73 In this study it is illustrated that if the dual node approach is properly implemented as well
74 as properly conceptualized, then the dual node approach is actually the more general, more elegant
75 as well as the more accurate approach. This is a significant finding particularly since this
76 contradicts the findings of other studies in which the common node is commonly regarded as a
77 more general and more elegant approach [Dawson, 2008; Kollet and Maxwell, 2006; Liggett *et al.*,
78 2012; Liggett *et al.*, 2013]. To arrive at a properly implemented or consistent dual node approach
79 the dual node approach is derived from basic flow equations. Moreover, to develop and understand
80 the consistent approach, it is crucial to realize that the topmost subsurface nodes should ideally
81 represent values at the centroids of discrete control volumes. It is shown that the dual node
82 approach should not be conceptualized as a distinct interface across which an exchange flux is
83 computed. Instead the dual node approach should be interpreted as a one-sided finite difference
84 approximation of the vertical hydraulic gradient at the land surface in which the coupling length
85 is defined by the grid geometry. Moreover, whereas the consistent dual node approach is in
86 agreement with the principle of head continuity at the surface-subsurface interface, it can be shown
87 that the common node approach is not.

88 In this study the coupling approaches are considered for cell-centered as well as vertex-
89 centered finite difference schemes. Theoretical considerations as well as numerical experiments



90 indicate that the dual node approach when properly implemented is often more accurate as well as
91 more computationally efficient than the common node approach, particularly if the vertical
92 discretization is relatively coarse. This is an important finding because using a relatively coarse
93 vertical discretization is common practice in regional coupled surface-subsurface models [*Jones*
94 *et al.*, 2008; *Kollet and Maxwell*, 2008; *Srivastava et al.*, 2014]. The numerical experiments are
95 carried out with the model code DisCo [*de Rooij et al.*, 2013].

96 **2 Interpretation of nodal values**

97 As explained later on, a correct interpretation of nodal values is crucial for understanding the dual
98 and common node approach for coupling surface-subsurface flow. Moreover, both coupling
99 approaches depend on the configuration of surface and topmost subsurface nodes near the land
100 surface. This configuration depends on whether cell-centered or vertex-centered schemes are used.
101 In this study both type of schemes will be covered, but for simplicity only finite difference schemes
102 are considered.

103 In both cell-centered as vertex-centered schemes the flow variables such as the heads and
104 the saturation are computed on nodes. In vertex-centered schemes these nodes coincide with the
105 vertices of mesh, whereas in cell-centered schemes the nodes coincide with the cell centers. When
106 employing a finite difference scheme, nodal values correspond to the mean value within
107 surrounding discrete control volumes. In cell-centered finite difference schemes these discrete
108 volumes are defined by the primary grid cells. In vertex-centered finite difference schemes these
109 discrete volumes are defined by the dual grid cells. Ideally, the mean values in the discrete control
110 volumes are derived by applying the midpoint rule for numerical integration such that their
111 approximation is second-order accurate. Therefore, the nodal values should ideally represent



112 values at the centroid of the surrounding discrete control volume [Blazek, 2005; Moukalled *et al.*,
113 2016]. In that regard, a cell-centered finite difference scheme is thus more accurate than a vertex-
114 centered finite difference scheme. Namely, in cell-centered finite difference schemes the nodal
115 values always correspond to the centroids of the cell whereas in vertex-centered finite difference
116 schemes nodes and centroids (of the dual cells) do not coincide at model boundaries and in model
117 regions where the primary grid is not uniform. It is well-known that this mismatch between nodes
118 and centroids can lead to inaccuracies since the mean values within affected discrete volumes are
119 not computed by a midpoint rule [Blazek, 2005; Moukalled *et al.*, 2016].

120 Typically, vertex-centered schemes for simulating coupled surface-subsurface flow are
121 based on mass-lumped finite element schemes [Liggett *et al.*, 2012] and not on finite difference
122 schemes. However, with respect to coupling surface-subsurface flow there is actually no difference
123 between a mass-lumped finite element scheme and a vertex-centered finite difference scheme.
124 Similar as in vertex-centered finite difference schemes, the nodal values in mass-lumped finite
125 element schemes define the mean values inside dual grid cells [Zienkiewicz *et al.*, 2005].
126 Moreover, the coupling approaches establish one-to-one relations between surface and topmost
127 subsurface nodes which do not depend on whether a finite difference or a finite element approach
128 is being used. Thus, a less complicated vertex-centered finite difference scheme may be used to
129 provide insights in the coupling approaches as used in mass-lumped finite element schemes.

130 **3 Common node approach**

131 The common node approach defines a head continuity between the topmost subsurface nodes and
132 the surface nodes. This continuity requires that the topmost subsurface nodes and the surface nodes
133 are co-located at the land surface such that there exists a continuity in the elevation head. This



134 requirement is automatically full-filled in vertex-centered schemes. Figure 1c illustrates the
135 configuration of common nodes for vertex-centered schemes. This configuration is similar to the
136 configuration as used in HydroGeoSphere [Therrien *et al.*, 2010]. However, in cell-centered
137 schemes such as ParFlow the co-location of nodes is less straightforward. Also, the basic
138 explanation that the pressure head continuity is assigned at the top cell of the subsurface domain
139 at the boundary between the two domains [Kollet and Maxwell, 2006; Maxwell *et al.*, 2009; Sulis
140 *et al.*, 2010] is ambiguous since the location of the land surface with respect to the top cell is not
141 specified. Nonetheless, since ParFlow is a cell-centered scheme where the topmost subsurface
142 node is located at the center of the top cell, it follows that the surface node is located at the center
143 of the topmost subsurface cells as depicted in Figure 1a such that the land surface is located at the
144 center of the topmost subsurface cell. This is the correct configuration as applied in ParFlow
145 [personal communication Maxwell, R. in relation to previous work of the author [De Rooij *et al.*,
146 2012]]. It can be argued that the additional subsurface volumes that extent above the land surface
147 do not drastically affect the timing of runoff. Namely, once the topmost subsurface node reaches
148 fully saturated conditions, the amount of additional water that can be stored in those volumes is
149 relatively small as long as the specific storage assigned to the topmost cell is relatively small.

150 Since the location of the land surface in ParFlow is somewhat unclear, some studies have
151 inferred that ParFlow uses a completely different nodal configuration. For example, it has been
152 inferred that the topmost subsurface nodes in the ParFlow model are placed on top of the topmost
153 subsurface cell such that they are co-located with the surface nodes [Liggett *et al.*, 2013]. An and
154 Yu [An and Yu, 2014] infer that the surface and subsurface nodes are not co-located at all and the
155 surface nodes are located at the top face of the topmost subsurface cells and that the topmost
156 subsurface nodes are located at the center of the topmost subsurface cells.



157 Considering that nodal values represent ideally the mean values within discrete control
158 volumes as described in Section 2, it can be argued that the head continuity as implemented in the
159 common node approach is not in agreement with the physical principle of head continuity at the
160 land surface. Namely, the common node approach enforces a continuity between surface heads at
161 the land surface and the mean subsurface heads within the topmost subsurface discrete control
162 volumes which have a finite thickness. This is different from enforcing a continuity between
163 surface heads and subsurface heads within an infinitesimal thin subsurface layer directly below the
164 land surface. As such inconsistent behavior is expected when using the common node approach.
165 To effectively remove this inconsistency a very fine vertical discretization is required near the land
166 surface.

167 **4 Consistent dual node implementation**

168 Figure 1b and 1c illustrate the classical arrangement of surface and subsurface nodes in cell-
169 centered and vertex-centered finite difference schemes, respectively. Commonly, the dual node
170 approach is expressed in terms of an exchange flux q_e [LT^{-1}] computed as [Liggett *et al.*, 2012;
171 Panday and Huyakorn, 2004]:

$$172 \quad q_e = f_p \frac{K_z}{l} (h_s - h_{ss}) \quad (1)$$

173 where h_s and h_{ss} are the hydraulic heads [L] associated with the surface node and the topmost
174 subsurface node, respectively, f_p [-] the fraction of the interface that is ponded and l the coupling
175 length [L]. The ponded fraction of the interface is typically defined by a function that varies
176 smoothly between zero at the land surface elevation and unity at the rill storage height which
177 defines the minimum water depth for initiating lateral overland flow [Panday and Huyakorn,



178 2004]. In equation (1) the term $f_p K_z / l$ is commonly referred to as the first-order exchange
179 parameter, where first-order means that the exchange flux depends linearly of the hydraulic head
180 difference.

181 Typically, equation (1) is not derived as a numerical approximation of basic flow equations
182 that govern the exchange flux, but is presented a numerical technique to couple two different flow
183 domains [Ebel *et al.*, 2009; Liggett *et al.*, 2012]. Subsequently, the dual node approach is
184 conceptualized by interpreting equation (1) as an expression that describes groundwater flow
185 across a distinct interface separating the two flow domains [Ebel *et al.*, 2009; Liggett *et al.*, 2012;
186 Liggett *et al.*, 2013]. Evidently, if the coupling length is assumed to be a non-physical parameter,
187 then it follows that equation (1) cannot be derived from basic flow equations. In the following,
188 however, it is illustrated that the dual node approach can and should be derived from basic
189 equations that describe infiltration into a porous medium. This derivation is inspired by but slightly
190 different from the work of Morita and Yen [Morita and Yen, 2002].

191 Before deriving the dual node approach from equations that describe infiltration, it is
192 worthwhile to point out that above formulation of an exchange flux implies that infiltration only
193 occurs across the ponded fraction of the surface-subsurface interface. This is not correct, because
194 rainfall typically results in infiltration across non-ponded areas. Although this issue is not a crucial
195 problem since the ponded fraction will typically increase during rainfall, it is more elegant to
196 account explicitly for infiltration across non-ponded areas. This is relatively straightforward since
197 before ponding occurs the infiltration rate equals the rainfall rate if the rainfall rate is smaller than
198 the infiltrability and is limited to the infiltrability otherwise [Hillel, 1982] and such a computation
199 is also used by others [Morita and Yen, 2002]. In the approach presented here the surface cell can



200 be partially ponded whereas in the work of Morita and Yen [Morita and Yen, 2002] a surface cell
 201 is either ponded or non-ponded.

202 Using Darcy's Law, the infiltration rate at the ponded land surface $q_{s \rightarrow ss}$ [LT^{-1}] can be
 203 written as a function of the vertical subsurface hydraulic gradient at the land surface:

$$204 \quad q_{s \rightarrow ss} = \left(k_r K_z \frac{\partial h}{\partial z} \right) \Big|_{z=z_s} = K_z \frac{\partial h}{\partial z} \Big|_{z=z_s} \quad (2)$$

205 where h the hydraulic head [L], z the elevation head [L], k_r the relative hydraulic conductivity [-]
 206 K_z the saturated vertical hydraulic conductivity [LT^{-1}] and z_s the elevation head at the land surface.
 207 The relative hydraulic conductivity is unity because equation (2) applies to the ponded land surface
 208 which implies fully saturated conditions at the land surface (i.e. ponding means $p_s > 0$, where p_s is
 209 the pressure head at the surface). Similarly, the infiltrability [LT^{-1}], defined as the infiltration rate
 210 under the condition of atmospheric pressure [Hillel, 1982], can be written as:

$$211 \quad I = \left(k_r K_z \frac{\partial h}{\partial z} \right) \Big|_{z=z_s, p_s=0} = K_z \frac{\partial h}{\partial z} \Big|_{z=z_s} \quad (3)$$

212 The relative hydraulic conductivity is again unity because the saturation equals unity under
 213 atmospheric conditions ($p_s = 0$). The infiltration rate at non-ponded land surface $q_{atm \rightarrow ss}$ [LT^{-1}] can
 214 be expressed as:

$$215 \quad q_{atm \rightarrow ss} = \min(\max(I, 0), q_R) \quad (4)$$

216 where q_R is the effective rainfall rate (i.e. the infiltration rate is limited by either the infiltrability
 217 or the available effective rainfall rate). The total exchange flux across the surface-subsurface
 218 interface can now be written as:

$$219 \quad q_e = f_p q_{s \rightarrow ss} + (1 - f_p) q_{atm \rightarrow ss} \quad (5)$$



220 To approximate the vertical subsurface hydraulic gradient in equations (2) and (3), it is
221 crucial to recognize that according to the principle of head continuity at the land surface, the
222 surface hydraulic head at a surface node must also represent the subsurface head at the land surface
223 at that location. Thus, the surface hydraulic head can be used as a Dirichlet boundary condition for
224 the subsurface flow domain. Moreover, it is also crucial to recognize that since the subsurface
225 hydraulic heads at the topmost subsurface nodes are ideally associated with the centroids of the
226 topmost subsurface discrete control volumes, these head values do not represent values at the land
227 surface but at some depth below the land surface. Because the subsurface hydraulic heads at the
228 dual nodes can be and should be associated with a different elevation, the vertical subsurface head
229 gradient between the dual nodes can be approximated by a standard finite difference
230 approximation. If this approximation is being used to approximate the gradient at the land surface
231 in equations (2) and (3), then this approximation is by definition a one-sided first-order finite
232 difference. Defining the coupling length by $l = \Delta z$ where Δz is the difference in the mean elevation
233 head associated with the dual nodes, the infiltration rate and infiltrability can thus be computed
234 with the following one-sided finite difference approximation:

$$235 \quad K_z \left. \frac{\partial h}{\partial z} \right|_{z=z_s} \approx \frac{K_z}{l} (h_s - h_{ss}) \quad (6)$$

236 The above definition of the coupling length $l = \Delta z$ ensures a proper approximation of the vertical
237 gradient in elevation head at the land surface:

$$238 \quad \left. \frac{\partial z}{\partial z} \right|_{z=z_s} = \frac{\Delta z}{l} = 1 \quad (7)$$

239 Since nodal values in cell-centered scheme are located at the centroids of the cells, the coupling
240 length is simply given by $l = z_s - z_{ss}$. This value has been proposed by others [Panday and



241 *Huyakorn*, 2004]. However, in vertex-centered schemes the commonly used nodal configuration
242 near the surface is such that $z_s = z_{ss}$. If these elevation heads are used as the elevation heads at the
243 dual nodes then $\Delta z = z_s - z_{ss} = 0$. Since the coupling length must be greater than zero, the coupling
244 length cannot be defined as $l = \Delta z$. Indeed, the coupling length in vertex-centered schemes is
245 typically not related to grid structure [*Liggett et al.*, 2013]. However, if $\Delta z = 0$ and the coupling
246 length is some lumped-parameter greater than zero, then the dual node approach is inconsistent.
247 Namely, if $\Delta z = 0$ then the gradient in elevation head between the dual nodes equals zero. This
248 may seem correct as the nodes are co-located. However, if $z_{ss} = z_s$, then the physical principle of
249 head continuity implies that $p_{ss} = p_s$ must also hold. Moreover, even though the topmost
250 subsurface node is located at the land surface in a vertex-centered scheme, the elevation head at
251 this node should ideally correspond to the mean elevation head within the topmost subsurface
252 discrete control volume such that $z_{ss} < z_s$. This suggests that the topmost subsurface node should
253 be moved to the centroid of the topmost subsurface discrete volume. Although this is a possible
254 solution, the drawback of this solution is that the subsurface model ceases to be a purely vertex-
255 centered scheme. Moreover, such an operation cannot be performed in finite element schemes
256 since changing the nodal positions would change the elements. Therefore, an alternative solution
257 is proposed. To enforce $l = z_s - z_{ss}$ without affecting the relative positions of nodes in the
258 subsurface grid, the elevation of the surface nodes are changed according to $z_s = z_{ss} + l$ where l is
259 equals half the thickness of the topmost subsurface dual cell. This change does also not affect the
260 relative position of the nodes in the surface grid. The resulting nodal configuration is illustrated in
261 Figure 1d. In essence, the motivation behind this solution is that a more accurate approximation
262 the hydraulic gradient is more important than the actual elevation of the land surface. Indeed it can



263 be argued that the change in land elevation will not drastically affect the timing of runoff. Namely,
264 once the topmost subsurface node reaches fully saturated conditions, the amount of additional
265 water needed to reach the elevated land surface is minor as long as the specific storage assigned to
266 the topmost dual cell is relatively small.

267 It is crucial to observe that the proposed dual node implementation is not based on
268 assuming a distinct interface with a certain thickness between the subsurface and the surface.
269 Instead, the coupling length is to be interpreted as a distance between dual nodes that accounts for
270 the fact that the topmost subsurface nodal value ideally corresponds to a value below the land
271 surface. This distance is related to the vertical discretization near the land surface and as such does
272 not represent a non-physical parameter associated with a distinct interface separating the two
273 domains.

274 The common conceptualization of the dual node approach as a hydraulic separation by a
275 interface with a given thickness [Kollet and Maxwell, 2006; Liggett *et al.*, 2012; Liggett *et al.*,
276 2013], may arise if dual node approach is interpreted as a second-order central finite difference
277 approximation evaluated at the centre of a saturated layer with a thickness equal to the coupling
278 length. If in addition the topmost subsurface head values are taken as values at the land surface,
279 then it follows that the dual node approach introduces a distinct interface between the two flow
280 domains. However, as explained the topmost subsurface head values should not be taken as values
281 at the land surface but as values at some distance from the land surface, such that the interface
282 defined by the coupling length occupies the upper half of the topmost subsurface discrete control
283 volumes.

284 It is also worthwhile to explain in further detail that the dual node approach does not
285 account for the relative hydraulic conductivity near the land surface. This does not imply that the



286 subsurface near the land surface is saturated. Namely, saturation in the topmost subsurface discrete
287 volume is computed with the pressure head at the topmost subsurface node which may well be
288 below zero. It may appear that the vertical hydraulic conductivity between the dual nodes should
289 be computed by weighting the vertical hydraulic conductivities at the dual nodes, which would
290 result in a dependency on the relative hydraulic conductivity as long as the topmost subsurface
291 node is not fully saturated. However, no weighting is needed if the dual node approach is
292 understood as a one-sided finite difference evaluated at the land surface. Namely, the vertical
293 hydraulic conductivity at the land surface is readily available. This is a difference with respect to
294 the approach of Morita and Yen [Morita and Yen, 2002] who do use a weighting scheme.
295 Moreover, models typically apply upstream weighting to approximate the relative hydraulic
296 conductivities between nodes to avoid numerical instabilities [Forsyth and Kropinski, 1997]. Thus
297 even if weighting is applied, then the dependency of the computations between the dual nodes on
298 the relative hydraulic conductivity will automatically disappear as the upstream node is always
299 saturated.

300 To illustrate that the presented dual node approach exhibits consistent behaviour, the
301 necessary conditions for ponding due to excess infiltration and exfiltration are considered. In
302 general ponding starts when $q_R > I$ [Hillel, 1982]. Setting $q_R = I$, $p_s = 0$ and using $h = p + z$, it
303 follows from equation (6) and (7) that at the moment of ponding:

$$304 \quad p_{ss} = l \left(1 - \frac{q_R}{K_z} \right) \quad (8)$$

305 Ponding due to excess infiltration occurs if $q_R/K_z > 1$ and implies that saturation in the subsurface
306 starts from the top down [Hillel, 1982]. Using $q_R/K_z > 1$ it follows from equation (8) that ponding
307 due to excess infiltration occurs while $p_{ss} < 0$. This is reasonable since this value represents the



308 pressure head at a certain depth below the land surface. Namely, if saturation occurs from the top-
309 down then the saturation at a certain depth occurs later than saturation at the land surface. It is
310 noted that if the ratio q_R/K_z is greater than but close to unity or if the coupling length is very small,
311 then this condition becomes $p_{ss} \approx 0$. Once ponding starts the total flux rate between the dual nodes
312 equals $K_z((p_s - p_{ss})/l + 1)$. Top-down saturation requires that this flux exceeds the vertical
313 hydraulic conductivity. Reaching saturation at the topmost node ($p_{ss} = 0$) thus requires $p_s \geq 0$.
314 Thus, top-down saturation will occur after ponding is initiated. Ponding due to excess saturation
315 occurs if $q_R/K_z < 1$ and implies that saturation in the subsurface starts from the bottom up [Hillel,
316 1982]. Using $p_s = 0$, it follows from equation (8) that ponding due to excess saturation occurs while
317 $0 < p_{ss} < l$. Thus ponding starts after reaching fully saturated conditions at the topmost subsurface
318 node, which is again reasonable. Namely, the topmost subsurface node represents a value at a
319 certain depth below the surface and thus bottom-up saturation implies that this node reaches
320 saturation earlier than the surface. It is noted that if the ratio q_R/K_z is smaller than but close to
321 unity or if the coupling length is very small, then ponding occurs when $p_{ss} \approx 0$.

322 5 Comparison to other dual node implementations

323 To illustrate that it is crucial to account for the meaning of the values at the topmost subsurface
324 nodes, it is instructive to consider what happens if these values are not taken as the mean values
325 within discrete control volumes. As a first example, consider vertex-centered schemes where the
326 dual nodes are defined such that $z_{ss} = z_s$ as illustrated in Figure 2c. As discussed in Section 4 this
327 is inconsistent because it defines a zero gradient in elevation head between the dual nodes.
328 Nonetheless such schemes have been used in several models [Ebel *et al.*, 2009; Liggett *et al.*,



329 2012]. Since the vertical gradient in elevation head between the dual nodes is zero the total flux
330 rate after ponding now equals $K_z (p_s - p_{ss})/l$. Top-down saturation requires that this flux exceeds
331 the vertical hydraulic conductivity. Thus, reaching saturation at the topmost subsurface node (
332 $p_{ss} = 0$) requires $p_s > l$. Therefore, top-down saturation will not occur if runoff occurs and if the
333 surface water depths remains smaller than the chosen coupling length. Indeed, it has been pointed
334 out in other studies that the coupling length should be smaller than the rill storage height [*Delfs et*
335 *al.*, 2009; *Liggett et al.*, 2012]. The zero vertical gradient in elevation head between the dual nodal
336 also means that the required condition for ponding now becomes $p_{ss} = -lq_R/K_z$. This implies that
337 ponding due to excess saturation occurs while the topmost subsurface node is not yet saturated.

338 A second example is the dual node approach for cell-centered schemes as implemented in
339 MODHMS which uses an adapted pressure-saturation relationship for the topmost subsurface
340 nodes such that the topmost subsurface node only becomes fully saturated if hydraulic head at the
341 node rises above the land surface [*Liggett et al.*, 2013]. Since the topmost subsurface heads are
342 associated with the cell centroid, this dual node scheme defines a unit gradient in elevation head
343 at the land surface. However, the saturation value at the topmost node is associated with a location
344 at the land surface and not with the centroid of a discrete control volume. This has undesirable
345 consequences. Namely, saturating the topmost subsurface node ($p_{ss} = l$) due to excess infiltration
346 requires that $p_s > l$. Indeed, when simulating excess infiltration with MODHMS, a very small
347 coupling length is needed to simulate top-down saturation due to excess infiltration. [*Gaukroger*
348 *and Werner*, 2011; *Liggett et al.*, 2013]. It can also be shown that ponding due to excess saturation
349 occurs while $0 < p_{ss} < l$. But, because of the adapted pressure-saturation relationship this means
350 that ponding starts while the topmost subsurface node is not yet saturated. Comparing these results



351 with the results for the consistent dual node implementation, it is clear that the adapted pressure-
352 saturation relationship has undesirable consequences.

353 The above inconsistent implementations of the dual node approach have been used in several
354 studies to compare the dual node approach with the common node approach [*Liggett et al.*, 2012;
355 *Liggett et al.*, 2013]. Such studies indicate that the dual node approach is typically only competitive
356 with the common node approach in terms of accuracy once the coupling lengths are very small.
357 The requirement for very small coupling lengths, however, are a direct consequence of using
358 inconsistent dual node approaches. Namely, by choosing very small coupling lengths these
359 inconsistencies are to some extent minimized. At best this minimization results in schemes that
360 mimic the common node approach. However, as discussed, the common node approach is also
361 inconsistent since it is not in agreement with the physical principle of a head continuity at the
362 surface-subsurface interface. Since current views on how the coupling approaches compare are
363 based on inconsistent dual node approaches, it is imperative to re-evaluate how the dual and
364 common node approaches compare if the dual node approach is properly implemented.

365 Considering how the dual and the common node approach compare it is also crucial that the
366 dual node approach is not to be conceptualized as a hydraulic separation between the flow domains
367 in the form of a saturated interface. Namely, this conceptualization is often deemed a serious
368 drawback of the dual node approach, since there is no evidence of such a distinct interface.
369 Moreover, misconceptions about the coupling approaches can result in confusion. For example, in
370 their paper An and Yu [*An and Yu*, 2014] reject the idea of using the dual node based on its classical
371 conceptualization as a saturated interface and argue that their model is based on the approach
372 proposed by Kollet and Maxwell [*Kollet and Maxwell*, 2006]. However, in their finite volume
373 model the surface and subsurface nodes are not co-located. As such their coupling approach is,



374 contrary to the claim of the authors, a dual node approach. This misunderstanding is probably also
375 related to aforementioned difficulties in inferring the nodal configuration as used in ParFlow.
376 Nonetheless, their approach is actually a properly implemented dual node approach practically
377 similar to the one proposed in this paper. Interestingly, the model of An and Yu [*An and Yu, 2014*]
378 is less sensitive to the vertical discretization near the land surface in comparison to ParFlow
379 However, since An and Yu were convinced that they followed the same coupling approach as
380 ParFlow they hypothesized that the difference in performance was probably related to using
381 irregular grids instead of orthogonal grids as in ParFlow [*An and Yu, 2014*]. However, if this
382 difference is instead due to using a different coupling approach, then this would be an indication
383 that a dual node approach is less sensitive to the vertical discretization near the land surface. This
384 reinforces the idea that it is desirable to reconsider the comparison between the two coupling
385 approaches.

386 **6 Numerical experiments**

387 To compare the coupling schemes in terms of accuracy and computational efficiency numerical
388 experiments are presented. These experiments are carried out with the model code DisCo which
389 can simulate coupled surface-subsurface flow using a fully implicit or monolithic scheme [*de Rooij*
390 *et al., 2013*]. This means that the linearized surface and subsurface flow equations are combined
391 into a single matrix system. An adaptive error-controlled predictor-corrector one-step Newton
392 scheme [*Diersch and Perrochet, 1999*] is used in which a single user-specified parameter controls
393 the convergence as well the time stepping regime. It is assumed that by using the same error norms
394 and the same model parameters that control the time-stepping, the simulations results as obtained
395 by different coupling approaches can be compared fairly in terms of accuracy and efficiency. For



396 brevity further details about the model are not discussed here and can be found elsewhere [*de Rooij*
397 *et al.*, 2013].

398 Table 1 lists the abbreviations used in the figures to distinguish between the coupling
399 approaches, to distinguish between cell-centered and vertex-centered schemes and to distinguish
400 between models based on a uniform primary grid and grids that use a very thin primary top cell.
401 The thickness of this top cell equals the thickness of the primary cells in the finest uniform grids.
402 In models containing this thin layer of cells the vertical discretization below the thin layer is based
403 on the coarsest uniform grids. Further details about the discretizations are given in the figures.

404 The presented experiments focus mainly on the comparison between the consistent dual
405 node approach and the common node approach. Inconsistent dual node implementations based on
406 a zero hydraulic head gradient between the dual nodes are only considered for relatively coarse
407 vertical discretizations to illustrate their short-comings vis-à-vis the consistent dual node approach.
408 It is noted, that although these schemes are commonly used in vertex-centered schemes, for the
409 purpose of this study they have also been implemented in the cell-centered schemes by using the
410 nodal configuration depicted in Figure 1a. The scheme with an adapted pressure-saturation
411 relationship is not considered.

412 **6.1 Soil column problems**

413 These simulation scenarios consider infiltration into a vertical soil column and are inspired by
414 scenarios as studied by Liggett et al. [*Liggett et al.*, 2012; *Liggett et al.*, 2013]. In the simulation
415 scenarios rainfall is applied to a soil column with a height of 5 m. Initial conditions are defined by
416 $h = 0$ m. The saturated conductivity is 1.0608 md^{-1} . The porosity is 0.41 and the specific storage
417 is 10^{-4} m^{-1} . The van Genuchten parameters are given by $s_r = 0.387$, $s_s = 1.0$, $\alpha = 7.5 \text{ m}^{-1}$ and $n =$
418 1.89.



419 For the first two scenarios a constant head boundary of $h = 0$ m is applied at the bottom of
420 the column and the flux rate applied to the top of the soil column exceeds the saturated conductivity
421 of the soil column, resulting in runoff due to excess infiltration. In the first scenario the applied
422 flux rate is 1.1 md^{-1} . Figure 2 and 3 illustrates the simulated runoff and the number of Newton
423 steps for this scenario, respectively. Figure 4 illustrates the simulated runoff for the second
424 scenario in which the flux rate is 10.608 md^{-1} . It is noted that figure 4 does not display the results
425 at later times when a steady-state is reached. However, to show the differences in results around
426 the timing of ponding only a limited time period is displayed. Figure 5 illustrates the number of
427 Newton steps for the second scenario. For the second scenario, Figure 6 compares the evolution in
428 water depth between the common node approach and the dual node approach when using a
429 relatively coarse vertical discretization and a cell-centered scheme.

430 To compare the different coupling approaches when simulating excess saturation, a third
431 scenario is considered. The model setup is exactly the same as before, except that the effective
432 rainfall rate is set to 0.5 md^{-1} and that the bottom boundary is changed into a no-flow boundary.
433 The simulated runoff is depicted in Figure 7. Figure 8 shows the total number of Newton steps
434 during the model runs. Figure 9 compares the evolution in water depth between the common node
435 approach and the dual node approach when using a relatively coarse vertical discretization and a
436 cell-centered scheme.

437 **6.2 Hillslope problems**

438 In the following the first two simulation scenarios consider hillslope problems as designed by Sulis
439 et al. [Sulis et al., 2010]. For the purpose of this study, a third scenario is considered in which the
440 initial and boundary conditions are different to create a flooding wave across an unsaturated
441 hillslope. The problems consist of a land surface with a slope of 0.05 which is underlain by a



442 porous medium. The domain is 400 m long and 80 m wide. The subsurface is 5 m thick. In the
443 direction of the length and in the direction of the width the discretization is 80 m. Different vertical
444 discretizations are considered. The van Genuchten parameters are given by $s_r = 0.2$, $s_s = 1.0$, $\alpha = 1$
445 m^{-1} and $n = 2$. The porosity is 0.4 and the specific storage is 10^{-4} . The Manning's roughness
446 coefficients are given by $3.3 \times 10^{-4} \text{ m}^{-1/3} \text{ min}$. The surface flow domain has a zero-gradient outflow
447 condition. For the first two simulation scenarios the domain is recharged with an effective rainfall
448 rate of $3.3 \times 10^{-4} \text{ m/min}$ for a duration of 200 minutes and the initial water table depth is at a depth
449 of 1.0 m below the land surface.

450 The first scenario considers excess infiltration and the saturated hydraulic conductivity
451 equals $6.94 \times 10^{-6} \text{ m/min}$. Figure 10 and 11 show the simulated runoff and the number of Newton
452 steps, respectively. For the second scenario which considers excess saturation, the saturated
453 conductivity equals $6.94 \times 10^{-4} \text{ m/min}$. Figure 12 and 13 illustrates the simulated runoff and the
454 number of Newton steps, respectively. In the third scenario a surface water flood wave crossing
455 the hillslope in the downhill direction is simulated by applying a Neumann boundary condition of
456 $1.0 \text{ m}^3/\text{s}$ to the surface nodes with the highest elevation. The initial water table is located at a depth
457 of 1.5 m. The vertical saturated hydraulic conductivity equals $6.94 \times 10^{-6} \text{ m/min}$. Figure 14
458 illustrates the differences in simulated runoff and Figure 15 illustrates the number of Newton steps
459 of the model runs. Figure 16 compares the evolution in water depth on the surface nodes as well
460 as the time step sizes between the common node approach and the dual node approach when using
461 a relatively coarse vertical discretization and a cell-centered scheme.



462 7 Discussion

463 7.1 Accuracy

464 Considering the simulation of vertical flow through the unsaturated zone, a relatively fine vertical
465 discretisation is needed to simulate sharp saturation fronts with the Richards' equation [*Pan and*
466 *Wierenga, 1995; Ross, 1990*]. A relatively fine vertical discretisation also implies that the common
467 node approach will be in close agreement with the physical principle of head continuity along the
468 surface-subsurface interface. Finally, if the vertical discretisation is relatively small then the
469 coupling length for the consistent dual node approach is also small and this implies that the dual
470 node approach mimics the common node approach. Therefore, it is expected that the coupling
471 approaches will give similar and accurate results if the vertical discretization is sufficiently fine.
472 Indeed, the simulations results indicate that a relatively fine and uniform vertical discretization
473 yields similar results for the common node approach as well as for the consistent dual node
474 approach (Figure 2a, 4a, 5a, 7a, 10a, 12a and 14a). The simulation results based on the finest
475 vertical discretization may thus be taken as reference solutions that enables a comparison of the
476 coupling approaches when a coarser vertical discretization is used. This is an important issue,
477 because using a relatively coarse vertical discretization is common practice in regional coupled
478 surface-subsurface models [*Jones et al., 2008; Kollet and Maxwell, 2008; Srivastava et al., 2014*].

479 7.1.1 Excess saturation

480 The simulation results of runoff due to excess saturation as obtained by the common node approach
481 and the consistent dual node approach illustrate that simulating excess saturation runoff is not
482 significantly affected by the vertical discretization (Figure 7 and 12). This is because the time
483 needed to reach fully saturated conditions in the subsurface is a simple function of the flow
484 boundary conditions and the initial water content. It is thus expected that the vertical discretization



485 does not significantly affect the simulation of excess saturation. Although the vertical
486 discretization may affect the computed initial water content, this effect is usually negligible. It has
487 been found in other studies that the vertical discretization has little effect on simulated runoff due
488 to excess saturation [Sulis *et al.*, 2010].

489 As described in Section 4, when using the consistent dual node approach, ponding due to
490 excess saturation occurs when $0 < p_{ss} < l$. Thus at the moment of ponding the hydraulic head at
491 the topmost subsurface node is generally below the land surface. When using the common node
492 approach, the hydraulic head at the topmost subsurface node is at the land surface at the moment
493 of ponding. However, if the specific storage is relatively small, then the timing of runoff will be
494 similar for both coupling approaches. Both approaches are thus expected to yield similar and
495 reasonably accurate results even when the vertical discretization is relatively coarse. Indeed, the
496 simulation results indicate that there is little difference between the common node approach and
497 the consistent dual node approach (Figure 7 and 12).

498 As indicated in figure 7d, when using an inconsistent dual node approach, the timing of
499 runoff may be underestimated unless a very small coupling length is being used. As discussed in
500 section 5 this is expected.

501 **7.1.2 Excess infiltration**

502 When simulating excess infiltration the common node approach requires fully saturated conditions
503 at the topmost subsurface node for ponding to occur. This is a direct consequence of the head
504 continuity between the surface nodes and the topmost subsurface nodes. However, top-down
505 saturation associated with excess infiltration implies that reaching fully saturated conditions in the
506 topmost subsurface discrete volumes should requires more time than reaching fully saturated
507 conditions in the very near surface, especially if the vertical discretization is relatively coarse. It is



508 thus expected that the common node approach delays runoff and this delay increases for a coarser
509 vertical discretization. In addition, if the saturation fronts are less sharp due to a relatively coarse
510 vertical discretization, it takes more time to reach saturated conditions at the common node. This
511 will further delay runoff. Indeed, the simulation results indicate clearly that runoff is delayed when
512 using the common node approach, particularly if the vertical discretization is relatively coarse
513 (Figure 2, 4, 10 and 14). It has also been found in other studies that the common node approach
514 delays runoff due to excess infiltration if the vertical discretization is relatively coarse [*Sulis et al.*,
515 2010]. The overestimation of the infiltration associated with the delay in runoff may result in runoff
516 due to excess saturation even if the applied flux rate should result in runoff due to excess
517 infiltration. This is illustrated in Figure 10c for the model run based on a cell-centered scheme and
518 the common node approach. This Figure illustrates that overestimating the infiltration can yield a
519 distinctive higher peak in runoff. Comparing this peak with the runoff responses in Figure 12, it is
520 clear that this model run simulates runoff due to excess saturation

521 In comparison, the consistent dual node displays more desirable behaviour. Namely, as
522 explained in Section 4, ponding due to excess infiltration occurs before reaching fully saturated
523 conditions at the topmost subsurface node which is arguably more correct if saturation occurs from
524 the top-down, particularly if the vertical discretization is relatively coarse. When using the
525 consistent dual node approach, the moment of ponding depends on the computation of the
526 infiltrability. A relatively coarse vertical discretization may result in an underestimation of the
527 vertical pressure gradient at the land surface. This is because in a soil close to hydrostatic
528 conditions the pressure heads increase with depth. Therefore the infiltrability during the early
529 stages of infiltration may be underestimated. If the applied flux rate is sufficiently large, then this
530 underestimation will result in an underestimation of the timing of runoff. It may be observed from



531 equation (8) that if the ratio q_R/K_z or the coupling length is sufficiently large, then ponding is
532 initiated immediately. Figure 10c and 14c illustrate that the timing of runoff can indeed be
533 underestimated due to a relatively coarse vertical discretization when using the consistent dual
534 node approach. However, during the later stages of infiltration the pressure head at the topmost
535 subsurface node will be underestimated due to the combined effect of an underestimated
536 infiltration rate and the overly diffused saturation fronts. This results in an overestimation of the
537 infiltration rate in the later stages. Thus at some time after ponding has started, it is expected that
538 the amount of runoff is underestimated. Contrary to the common node approach, however, there
539 will be a time at which runoff is simulated correctly (Figure 10c and 14c).

540 If the applied flux rate is not sufficiently large, then the underestimated infiltrability in the
541 early stages of infiltration will not be exceeded. In that case, the overly diffused saturation fronts
542 resulting from a relatively coarse vertical discretization will eventually lead to an underestimation
543 of pressure head at the topmost subsurface node and as such the infiltrability may be overestimated
544 at later times. Consequently, when using the consistent dual node approach the timing of runoff
545 due to excess infiltration may also be underestimated. As discussed in section 4 if the ratio q_R/K_z
546 goes to unity, then the consistent dual node approach behaves practically similar to the common
547 node approach. Indeed, Figure 2b which depicts a simulation with a relatively small ratio q_R/K_z
548 clearly illustrates that the timing of runoff may be underestimated when using the consistent dual
549 node approach. However, the delay in runoff as simulated by the consistent dual node approach
550 will only equal the delay in runoff as simulated by the common node approach in the limit when
551 q_R/K_z goes to unity. In general, if the consistent dual node approach delays runoff, this delay will
552 be smaller than the delay in runoff as simulated by the common node approach (Figure 2b).
553 Overall, regardless if the consistent dual node approach underestimates or overestimates the timing



554 of runoff, the simulation results indicate that the consistent dual node approach is generally less
555 inaccurate than the common node approach for simulating excess infiltration when using a
556 relatively coarse uniform vertical discretization.

557 As illustrated in Figure 2b, 4b, 10b and 14b, if the coupling approach and the vertical
558 discretization are identical and if the thin layer is absent, then the vertex-centered schemes are
559 more accurate with respect to the cell-centered schemes. This difference in accuracy results solely
560 from the fact the primary mesh is the same for both schemes. As such the vertical extent of the
561 topmost subsurface volumes is twice as small when using the vertex-centered scheme. This
562 difference in vertical grid resolution near the land surface explains the differences in accuracy
563 between the schemes.

564 When using a thin layer at the top of the model the common node approach and consistent
565 dual node approach provide similar simulation results as shown in Figure 2c, 4c, 10d and 14d. This
566 is expected, because the thin layer implies a small coupling length and as such the consistent dual
567 node approach mimics the common node approach. In essence, in schemes using the consistent
568 dual node approach the thin layer establishes a near head continuity between the dual nodes. If the
569 simulation results are compared to the models based on the coarsest uniform discretization (Figure
570 2b, 4b, 10c and 14c), it is observed that adding a thin layer has only a positive effect on the cell-
571 centered schemes based on the common node approach. This positive effect is explained by the
572 fact that due to the thin layer the common node approach is in almost full agreement with the
573 principle of head continuity at the land surface. Vis-à-vis the corresponding model without a thin
574 layer, the thin layer has a negligible effect on the cell-centered scheme based on the consistent dual
575 node approach. This is because the thin layer establishes a head continuity between the dual nodes
576 and the topmost subsurface node and the adjacent subsurface node below act like the dual nodes



577 in the model without the thin layer. The thin layer has also a negligible effect on the vertex-centered
578 scheme based on the common approach. In this case the thin layer establishes a near head
579 continuity between the topmost subsurface node and the adjacent node below and ponding due to
580 excess infiltration will require almost fully saturated conditions in the two topmost subsurface
581 volumes. The sum of these two volumes is equal to the topmost volume in the model without the
582 thin layer and therefore the effect of the thin layer is minimal. In a vertex-centered scheme based
583 on the consistent dual node approach, the thin layer has a clear negative effect. In essence the head
584 continuity between the dual nodes removes the benefits of using the consistent dual node approach
585 and contrary to the cell-centered scheme based on the consistent dual node approach the topmost
586 subsurface node and the adjacent subsurface node below do not act like the dual nodes in the model
587 without the thin layer. This is because the thin layer creates a non-uniform primary mesh in which
588 the subsurface node directly below the topmost subsurface node is not located at the centroid of
589 its associated dual cell.

590 As indicated in figure 2d and 4d, when using an inconsistent dual node approach, the runoff
591 is overestimated unless a very small coupling length is being used. As discussed in section 5, this
592 is expected.

593 **7.2 Computational efficiency**

594 During the early stages of ponding the rates at which the water depths are changing can be
595 relatively fast as the applied flux rates on the land surface are possibly quite large. Typically, a
596 numerical model with adaptive time-stepping will decrease the time step size at the moment of
597 ponding to handle the non-linear flow terms and the high rates of change in water depth. Since a
598 higher infiltration rate at the moment of ponding results in lower initial rates of change in water



599 depth, it is expected that the most efficient coupling approach is characterized by a higher
600 infiltration rate at the moment of ponding.

601 The computational efficiency of the schemes is measured in terms of the number of Newton
602 steps. The number of Newton steps equals the number of times that the linearized system of
603 equations is solved and this number depends on the time step sizes as well as the number of failed
604 Newton steps.

605 **7.2.1 Excess saturation**

606 When simulating excess saturation the subsurface is fully pressurized at the moment of ponding
607 and can only accommodate additional water volumes by means of the specific storage. As such
608 the column will be close to hydrostatic conditions at the moment of ponding. When using the
609 common node approach this implies that the hydraulic gradient between the common node and the
610 adjacent subsurface node below is very close to zero. When using the consistent dual node
611 approach ponding due to excess saturation occurs when $0 < p_{ss} < l$. Thus, at the moment of
612 ponding the hydraulic head at the topmost subsurface node is generally still below the land surface.
613 This means that the infiltration rate at the moment of ponding as computed by the consistent dual
614 node approach is higher in comparison to the rate as computed by the common node approach. It
615 is thus expected that the consistent dual node approach is more efficient when simulating excess
616 saturation. Indeed, Figure 8 and 13 illustrate that, when simulating excess saturation, the
617 consistent dual node approach is more efficient than the common node approach. Figure 10
618 illustrates the pressure heads on the nodes near the land surface as simulated by the models based
619 on the cell-centered scheme and the coarsest vertical discretization. As illustrated, the pressure
620 head gradient governing the infiltration rate at the moment of ponding is larger when using the
621 consistent dual node approach and consequently the rate of change in water depth is smaller.



622 7.2.2 Excess infiltration

623 As discussed in section 7.1.2, in comparison to the consistent dual node approach, the common
624 node approach yields a later time of ponding due to excess infiltration. Since saturation fronts in a
625 homogeneous medium become more diffused with time, it follows that the common node approach
626 yields a smaller infiltration rate at the moment of ponding. Namely, if the saturation fronts are
627 more diffused, then the pressure head gradient governing the infiltration rate is less sharp.
628 Therefore, it is expected that the common node approach is computationally less efficient than the
629 consistent dual node approach, particularly if ponding is significantly delayed. Figure 5 illustrates
630 clearly, that the consistent dual node approach can be more computationally efficient. For the
631 simulation scenario depicted in Figure 5, the consistent dual node approach is also more accurate.
632 Figure 4b illustrates that, compared to the consistent dual node approach, the common node
633 approach can result in a relatively high rate of change in runoff at the moment of ponding. This is
634 indicative of a relatively high initial rate of change in water depth at the moment of ponding. Figure
635 7 illustrates the pressure heads at the nodes near the land surface as simulated by the cell-centered
636 schemes based on the coarsest vertical discretization. It can be observed that the pressure head
637 gradient at the moment of ponding is larger when using the consistent dual node approach. This
638 implies a higher infiltration rate and a lower rate of change in water depth. Figure 11 also illustrates
639 that the consistent dual node approach is more efficient when handling the activation of ponding.
640 However, considering the entire simulation period, the dual node approach is not always more
641 efficient. As illustrated by Figure 11b and 11c, when the discretization is relatively coarse the
642 common node approach is sometimes more efficient during the later stages of the simulation.
643 However, in these cases the common node approach is only more efficient, because its inaccuracy



644 leads to an easier flow problem to be solved. Namely, the underestimation of runoff results in more
645 diffused saturation fronts in the subsurface.

646 Figure 2, shows that if the ratio q_R/K_z is relatively small, then the differences in
647 computational efficiency are relatively small. As discussed in section 4 this is because the
648 consistent dual node approach behaves very similar to the common node approach if the ratio q_R/K_z
649 is relatively small.

650 Another factor that affects the efficiency of the common node approach is that the delay in
651 ponding can act as an artificial barrier for a surface water wave advancing across an initially
652 unsaturated subsurface domain. The effect of this artificial barrier is that the front of the surface
653 water wave is steepened. This steepening of the surface wave front results in higher rates at which
654 the water depth is changing and is undesirable because it decreases the computational efficiency.
655 This is clearly illustrated in Figure 15. Figure 16 illustrates the evolution of water depth at the land
656 surface for the cell-centered schemes using the coarsest vertical discretization. As shown, the
657 common node approach delays and steepens the surface water front. This results in relatively high
658 rates of change in water depth at the moment of ponding. Consequently, the common node
659 approach is less efficient than the dual node approach. It is noted that for this scenario the
660 consistent dual node approach is more efficient as well as more accurate.

661 **8 Conclusions**

662 In this study it is shown that contrary to the common held view, the dual node approach if properly
663 implemented is actually the more general, the more elegant as well as the more accurate coupling
664 approach in comparison to the common node approach. This consistent dual node approach is
665 implemented in cell-centered as well as vertex-centered finite difference schemes.



666 The consistent dual node approach is derived from basic equations that govern infiltration
667 and infiltrability at the land surface using a one-sided finite differences approximation of the
668 vertical hydraulic gradient at the land surface. In both cell-centered as vertex-centered schemes
669 the coupling length is related to the grid geometry. As discussed, the dual node approach should
670 not be conceptualized as a distinct interface between the surface and the subsurface. Moreover,
671 this approach is in agreement with principle of head continuity along the land surface whereas the
672 common node approach is not, unless the vertical discretization is sufficiently fine.

673 Numerical experiment indicate that if the vertical discretization is relatively coarse, then
674 the consistent dual node approach is often less inaccurate as well as more computationally efficient
675 in comparison to the common node approach for simulating excess infiltration. For simulating
676 excess saturation both coupling approaches are more or less equally accurate, but the consistent
677 dual node approach was found to be more computationally efficient. Therefore, overall it can be
678 argued that the consistent dual node approach is to be preferred to the common node approach
679 unless the vertical discretization is sufficiently fine such that both approaches yield similar results.
680

681 **Acknowledgements**

682 This research was funded by the Carl. S. Swisher Foundation.

683

684 **References**

685 An, H., and S. Yu (2014), Finite volume integrated surface- subsurface flow modeling on
686 nonorthogonal grids, *Water Resources Research*, 50(3), 2312-2328.
687 Blazek, J. (2005), *Computational fluid dynamics: Principles and applications* *Computational fluid*
688 *dynamics: Principles and applications*, Elsevier.



- 689 Dawson, C. (2008), A continuous/discontinuous Galerkin framework for modeling coupled
 690 subsurface and surface water flow, *Computational Geosciences*, 12(4), 451-472.
- 691 De Rooij, R., W. Graham, and R. Maxwell (2012), A particle-tracking scheme for simulating
 692 pathlines in coupled surface-subsurface flows, *Advances in Water Resources*.
- 693 de Rooij, R., P. Perrochet, and W. Graham (2013), From rainfall to spring discharge: Coupling
 694 conduit flow, subsurface matrix flow and surface flow in karst systems using a discrete-continuum
 695 model, *Advances in Water Resources*, 61, 29-41.
- 696 Delfs, J. O., C. H. Park, and O. Kolditz (2009), A sensitivity analysis of Hortonian flow, *Advances
 697 in Water Resources*, 32(9), 1386-1395.
- 698 Diersch, H. J. G., and P. Perrochet (1999), On the primary variable switching technique for
 699 simulating unsaturated-saturated flows, *Advances in Water Resources*, 23(3), 271-301.
- 700 Ebel, B. A., B. B. Mirus, C. S. Heppner, J. E. VanderKwaak, and K. Loague (2009), First-order
 701 exchange coefficient coupling for simulating surface water-groundwater interactions: parameter
 702 sensitivity and consistency with a physics-based approach, *Hydrological Processes*, 23(13), 1949-
 703 1959.
- 704 Forsyth, P. A., and M. C. Kropinski (1997), Monotonicity considerations for saturated-unsaturated
 705 subsurface flow, *Siam Journal on Scientific Computing*, 18(5), 1328-1354.
- 706 Gaukroger, A. M., and A. D. Werner (2011), On the Panday and Huyakorn surface-subsurface
 707 hydrology test case: analysis of internal flow dynamics, *Hydrological Processes*, 25(13), 2085-
 708 2093.
- 709 Hillel, D. (1982), *Introduction to soil physics*, Academic press New York.
- 710 Jones, J. P., E. A. Sudicky, and R. G. McLaren (2008), Application of a fully-integrated surface-
 711 subsurface flow model at the watershed-scale: A case study, *Water Resources Research*, 44(3).
- 712 Kolditz, O., and H. Shao (2010), OpenGeoSys, Developer-Benchmark-Book, OGS-DBB 5.04,
 713 Helmholtz Centre for Environmental Research (UFZ).
- 714 Kollet, S. J., and R. M. Maxwell (2006), Integrated surface-groundwater flow modeling: A free-
 715 surface overland flow boundary condition in a parallel groundwater flow model, *Advances in
 716 Water Resources*, 29(7), 945-958.
- 717 Kollet, S. J., and R. M. Maxwell (2008), Capturing the influence of groundwater dynamics on land
 718 surface processes using an integrated, distributed watershed model, *Water Resources Research*,
 719 44(2).
- 720 Liggett, J. E., A. D. Werner, and C. T. Simmons (2012), Influence of the first-order exchange
 721 coefficient on simulation of coupled surface-subsurface flow, *Journal of Hydrology*, 414, 503-515.
- 722 Liggett, J. E., M. J. Knowling, A. D. Werner, and C. T. Simmons (2013), On the implementation
 723 of the surface conductance approach using a block-centred surface-subsurface hydrology model,
 724 *Journal of Hydrology*, 496, 1-8.
- 725 Maxwell, R., S. J. Kollet, S. G. Smith, C. S. Woodward, R. D. Falgout, I. M. Ferguson, C. Baldwin,
 726 W. J. Bosl, R. Hornung, and S. Ashby (2009), ParFlow user's manual, *International Ground Water
 727 Modeling Center Report GWMI*, 1(2009), 129p.
- 728 Morita, M., and B. C. Yen (2002), Modeling of conjunctive two-dimensional surface-three-
 729 dimensional subsurface flows, *Journal of Hydraulic Engineering-Asce*, 128(2), 184-200.
- 730 Moukalled, F., L. Mangani, and M. Darwish (2016), *The Finite Volume Method in Computational
 731 Fluid Dynamics*, Springer.
- 732 Pan, L., and P. J. Wierenga (1995), A transferred pressure head based approach to solve Richards
 733 equation for variably saturated soils, *Water Resources Research*, 31(4), 925-931.



- 734 Panday, S., and P. S. Huyakorn (2004), A fully coupled physically-based spatially-distributed
 735 model for evaluating surface/subsurface flow, *Advances in Water Resources*, 27(4), 361-382.
- 736 Ross, P. J. (1990), Efficient numerical methods for infiltration using Richards equation, *Water*
 737 *Resources Research*, 26(2), 279-290.
- 738 Srivastava, V., W. Graham, R. Munoz-Carpena, and R. M. Maxwell (2014), Insights on geologic
 739 and vegetative controls over hydrologic behavior of a large complex basin - Global Sensitivity
 740 Analysis of an integrated parallel hydrologic model, *Journal of Hydrology*, 519, 2238-2257.
- 741 Sulis, M., S. B. Meyerhoff, C. Paniconi, R. M. Maxwell, M. Putti, and S. J. Kollet (2010), A
 742 comparison of two physics-based numerical models for simulating surface water-groundwater
 743 interactions, *Advances in Water Resources*, 33(4), 456-467.
- 744 Therrien, R., R. G. McLaren, E. A. Sudicky, and S. M. Panday (2010), HydroGeoSphere-a three-
 745 dimensional numerical model describing fully-integrated subsurface and surface flow and solute
 746 transport (draft), Groundwater Simulations Group, University of Waterloo.
- 747 VanderKwaak, J. E. (1999), Numerical simulation of flow and chemical transport in integrated
 748 surface-subsurface hydrologic systems, University of Waterloo.
- 749 Weill, S., A. Mazzia, M. Putti, and C. Paniconi (2011), Coupling water flow and solute transport
 750 into a physically-based surface-subsurface hydrological model, *Advances in Water Resources*,
 751 34(1), 128-136.
- 752 Yeh, G.-T., D.-S. Shih, and J.-R. C. Cheng (2011), An integrated media, integrated processes
 753 watershed model, *Computers & Fluids*, 45(1), 2-13.
- 754 Zienkiewicz, O., R. Taylor, and J. Zhu (2005), *The finite element method: its basis and*
 755 *fundamentals*. 2005, edited, Butterworth-Heinemann.

756

757

758

abbreviation	meaning
cc	cell-centered
vc	vertex-centered
dn	dual node
cn	common node
TL	tiny layer

759

760 Table 1: Abbreviations as used in the figures.

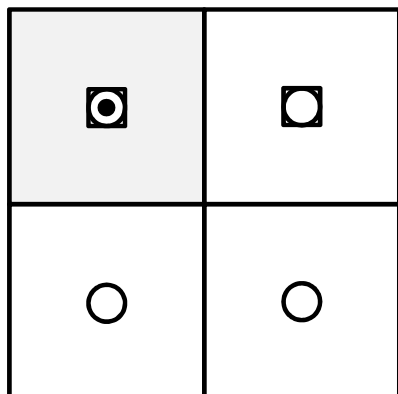
761

762



763

a)



764

765

766

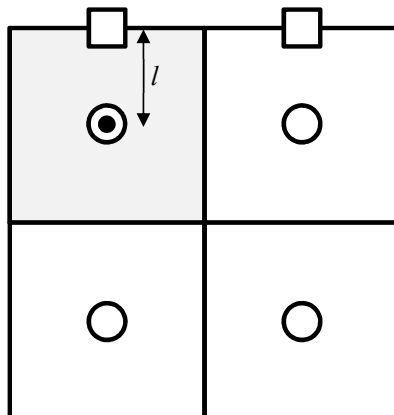
767

768

769

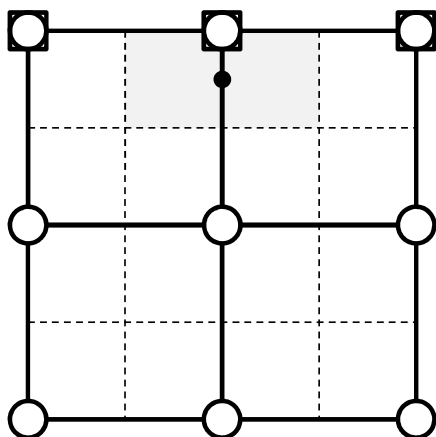
770

b)



771

c)



772

773

774

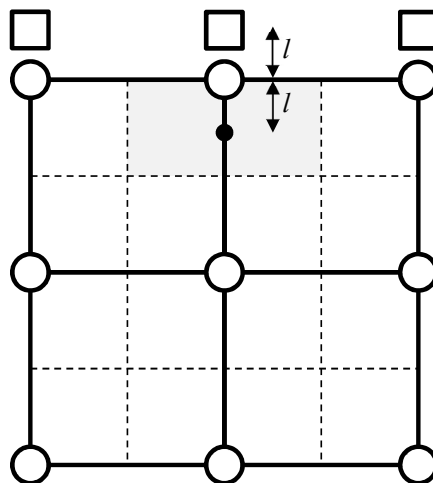
775

776

777

778

d)



779

780

781

782



783 Figure 1: a) Common nodes and co-located dual nodes in cell-centered schemes. b) Common nodes and
784 co-located dual nodes in vertex-centered schemes. c) Dual nodes in cell-centered schemes (not
785 col-located). d) Dual nodes in vertex-centered schemes (not co-located). The white squares and white
786 circles represent surface and subsurface nodes, respectively. The solid and dashed lines represent the
787 primary mesh and the dual mesh, respectively. The grey-shaded area is a topmost discrete volume as
788 associated with a topmost subsurface node. The black dot represents the centroid of this volume. The
789 coupling length l as depicted in this figure applies to the consistent dual node approach.

790

791

792

793

794

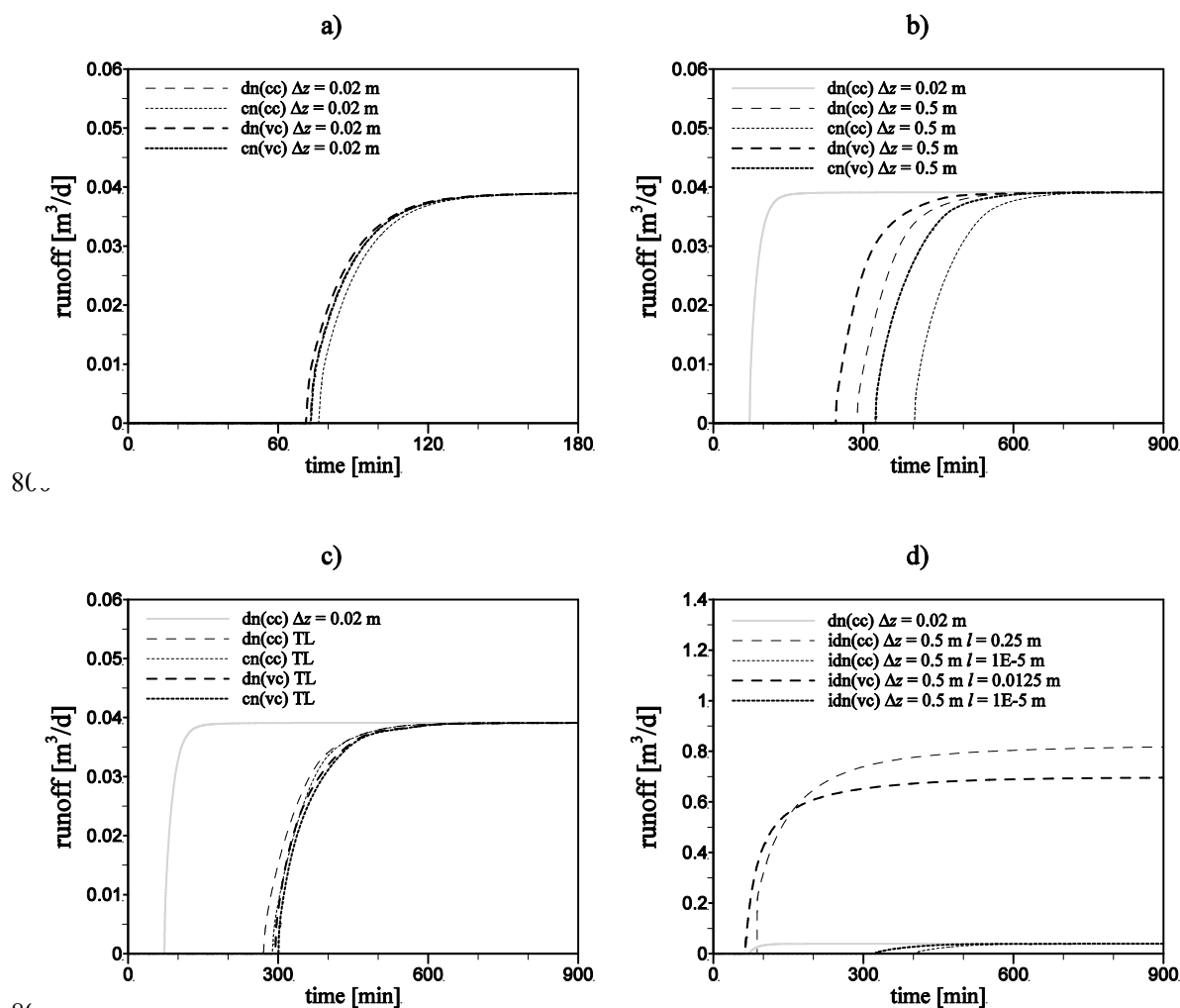
795

796

797

798

799



801

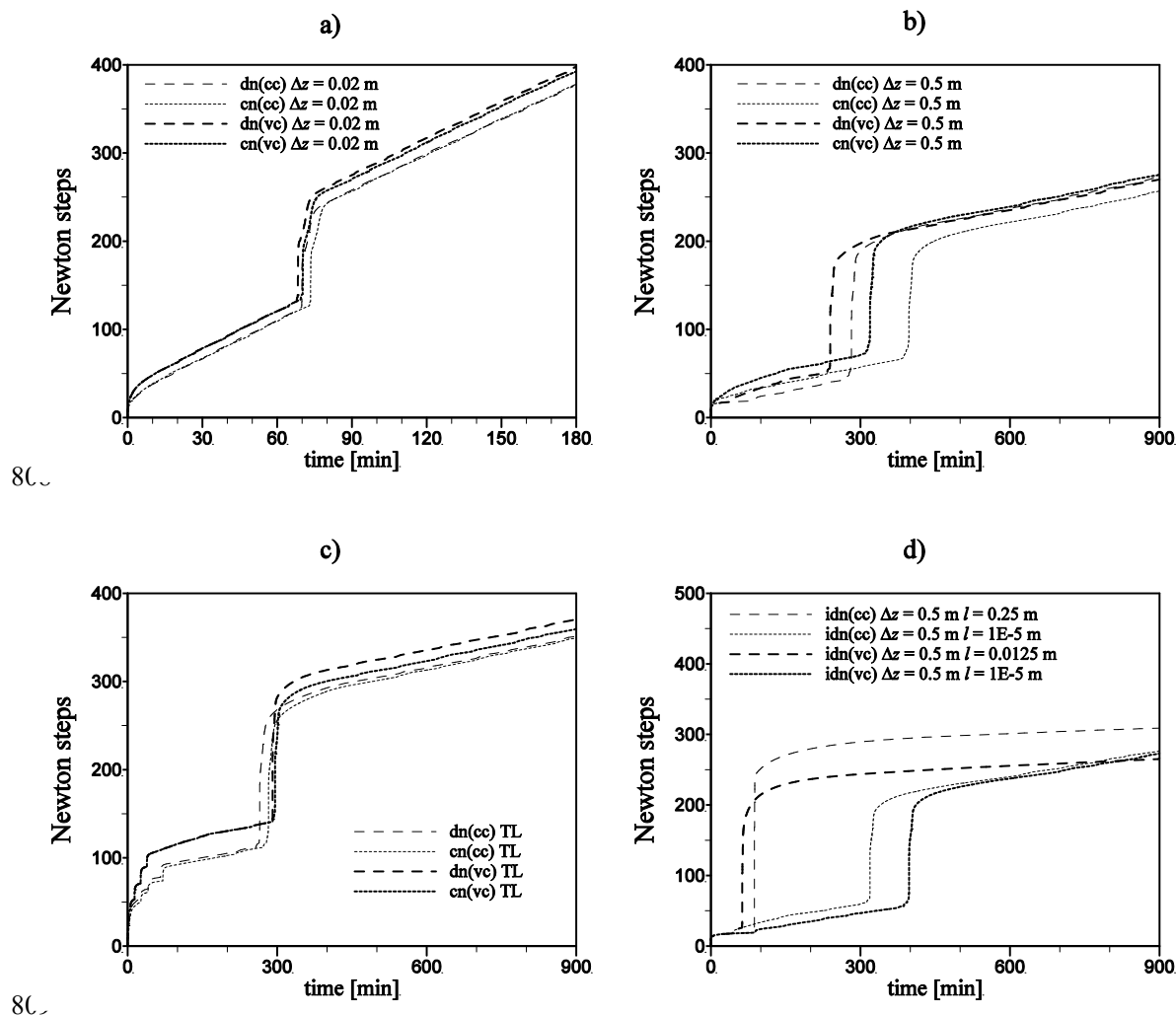
802 Figure 2: Simulated runoff for excess infiltration in a vertical soil column using different vertical
 803 discretizations ($q_R = 1.1 \text{ md}^{-1}$).

804

805

806

807



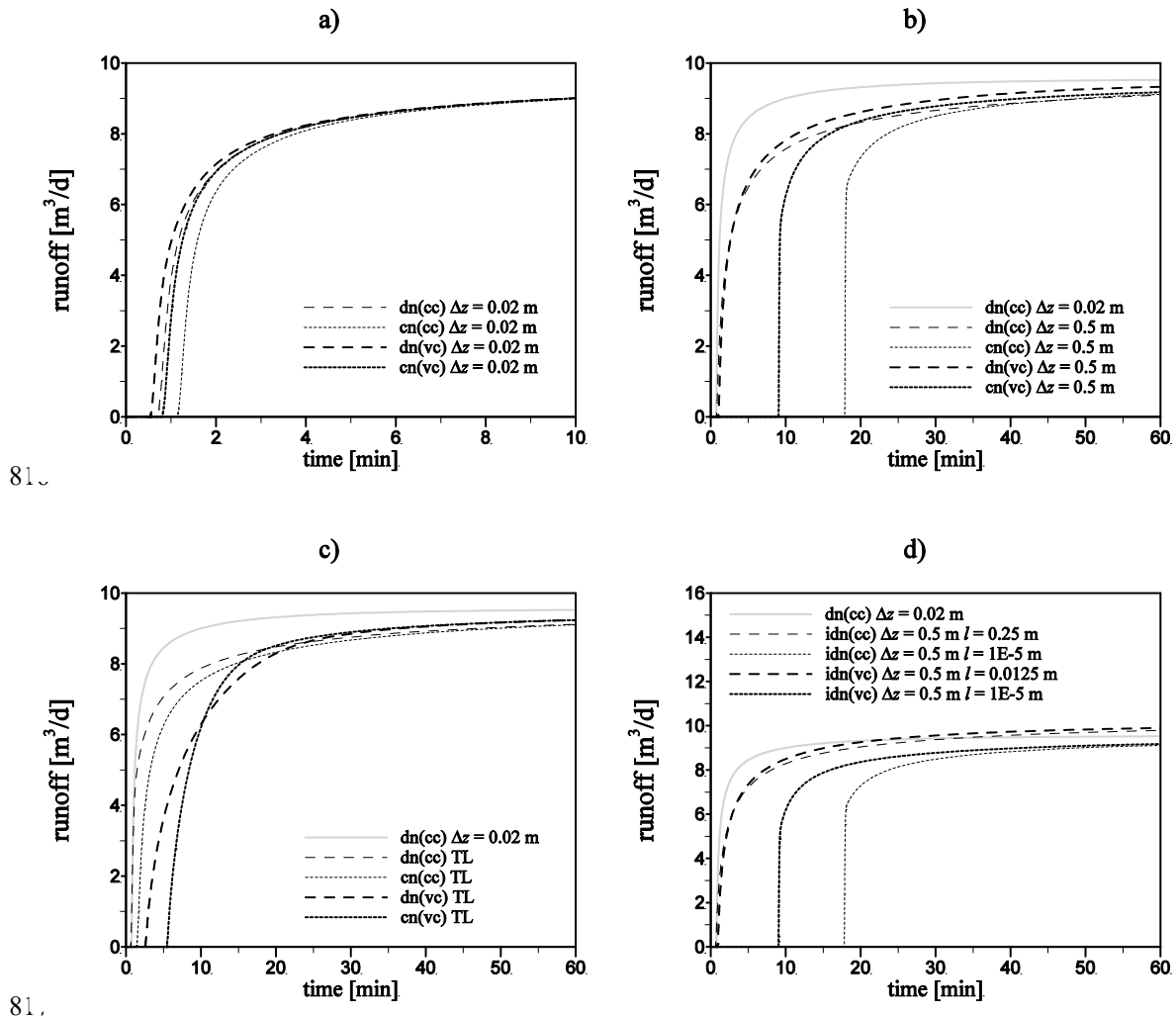
800
 810 Figure 3: Number of Newton steps for excess infiltration in a vertical soil column using different vertical
 811 discretizations ($q_R = 1.1 \text{ md}^{-1}$).

812

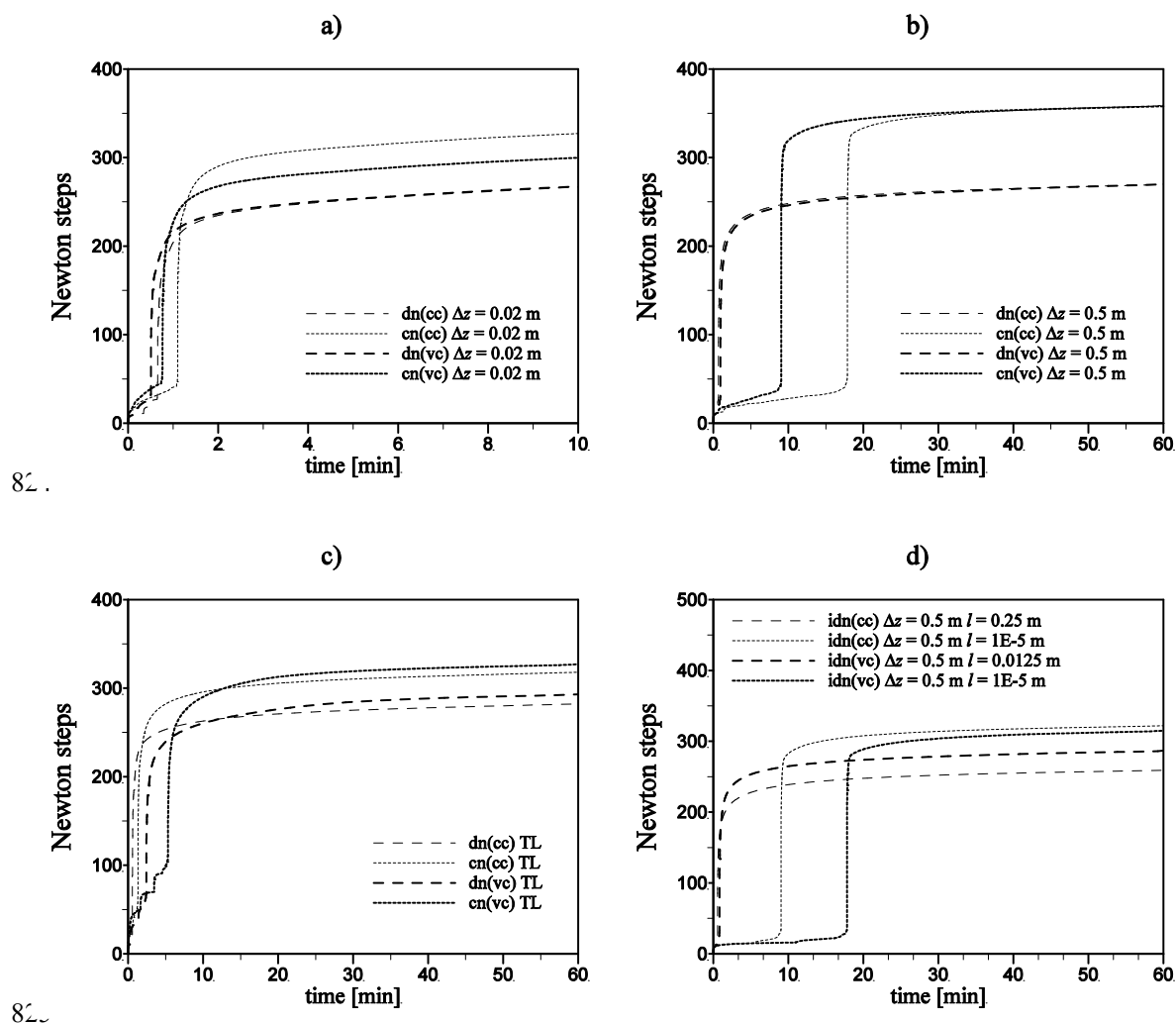
813

814

815



818 Figure 4: Simulated runoff for excess infiltration in a vertical soil column using different vertical
 819 discretizations ($q_R = 10.608 \text{ md}^{-1}$).



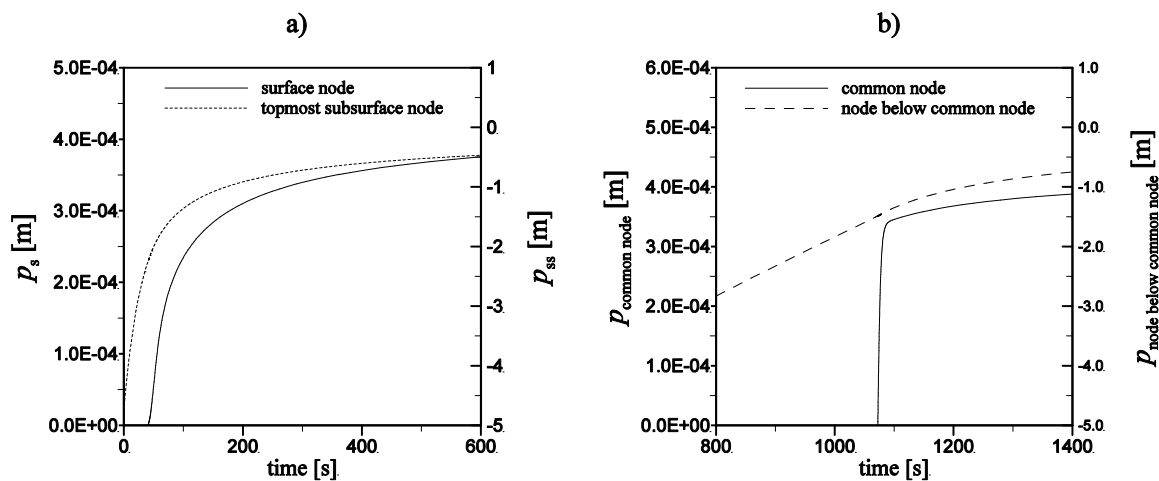
826 Figure 5: Number of Newton steps for excess infiltration in a vertical soil column using different vertical
 827 discretizations ($q_R = 10.608 \text{ md}^{-1}$).

828

829

830

831



832

833 Figure 6: Changes in pressure heads near the surface-subsurface interface for excess infiltration in a vertical
834 soil column ($q_R = 10.608 \text{ md}^{-1}$). Left: $dn(cc) \Delta z = 0.5 \text{ m}$. Right: $cn(cc) \Delta z = 0.5 \text{ m}$.

835

836

837

838

839

840

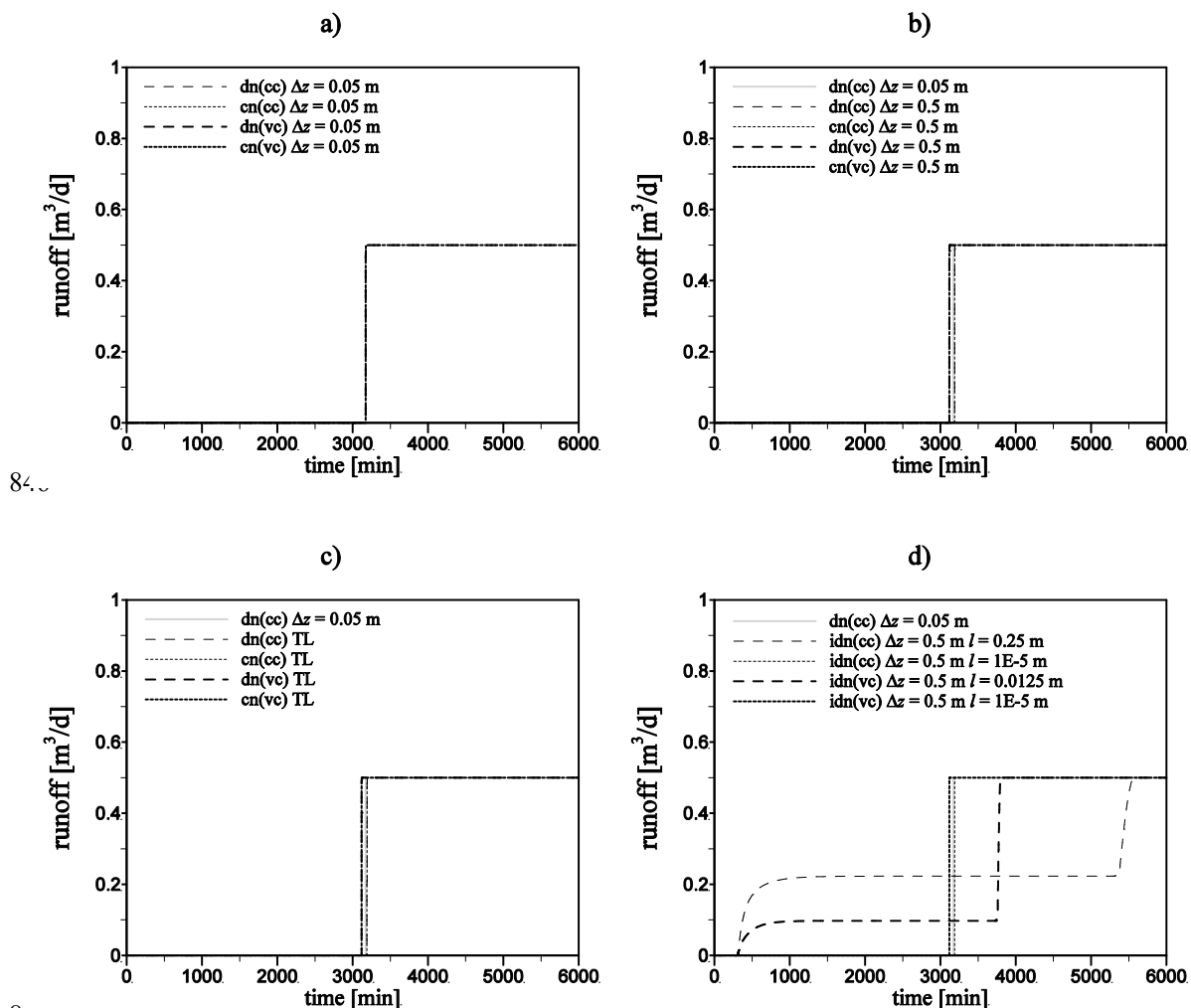
841

842

843

844

845



848 Figure 7: Simulated runoff for excess saturation in a vertical soil column using different vertical
 849 discretizations.

850

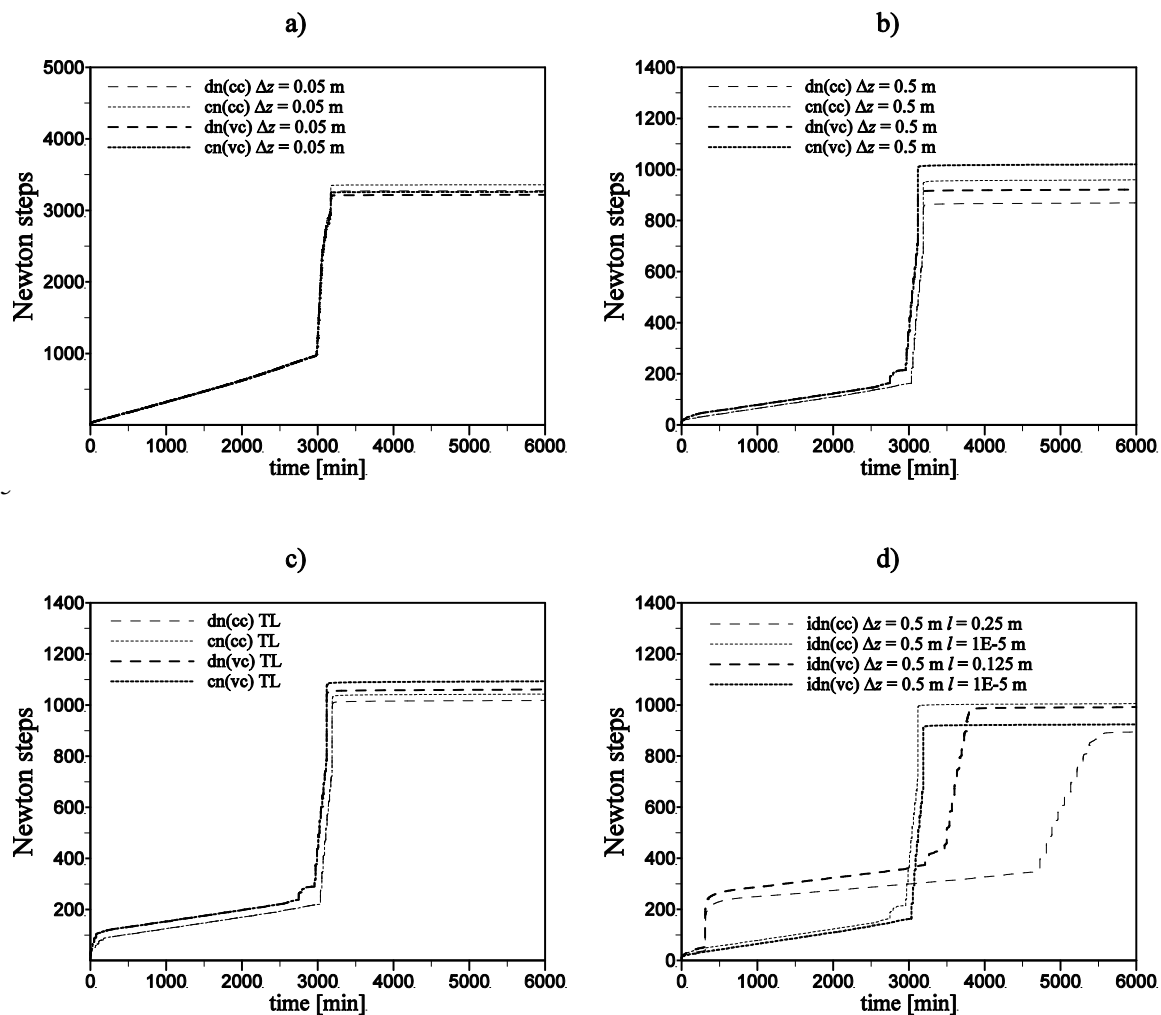
851

852

853



854

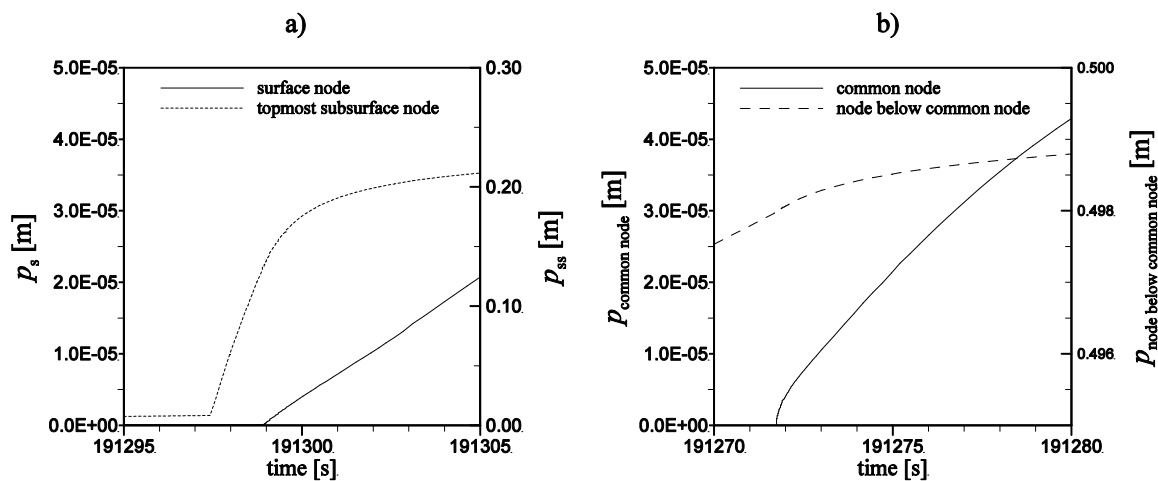


855

856

857 Figure 8: The total number of Newton steps for excess saturation in a vertical soil column using different
 858 vertical discretizations.

859



860

861 Figure 9: Changes in pressure heads near the surface-subsurface interface for excess saturation in a vertical
 862 soil column. Left: dn(cc) $\Delta z = 0.5$ m. Right: cn(cc) $\Delta z = 0.5$ m.

863

864

865

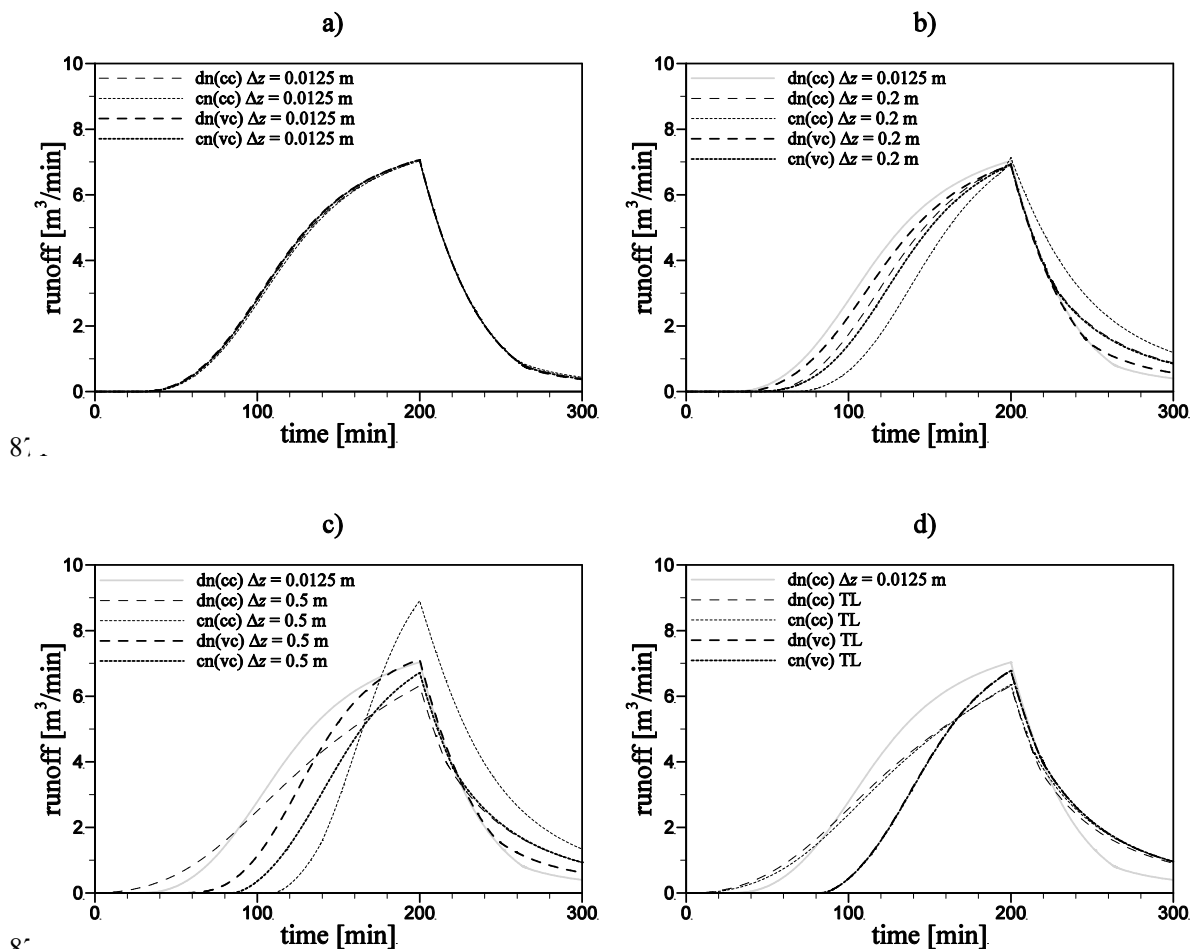
866

867

868

869

870



873 Figure 10: Outflow response for excess infiltration on a hill slope using different vertical discretizations.

874

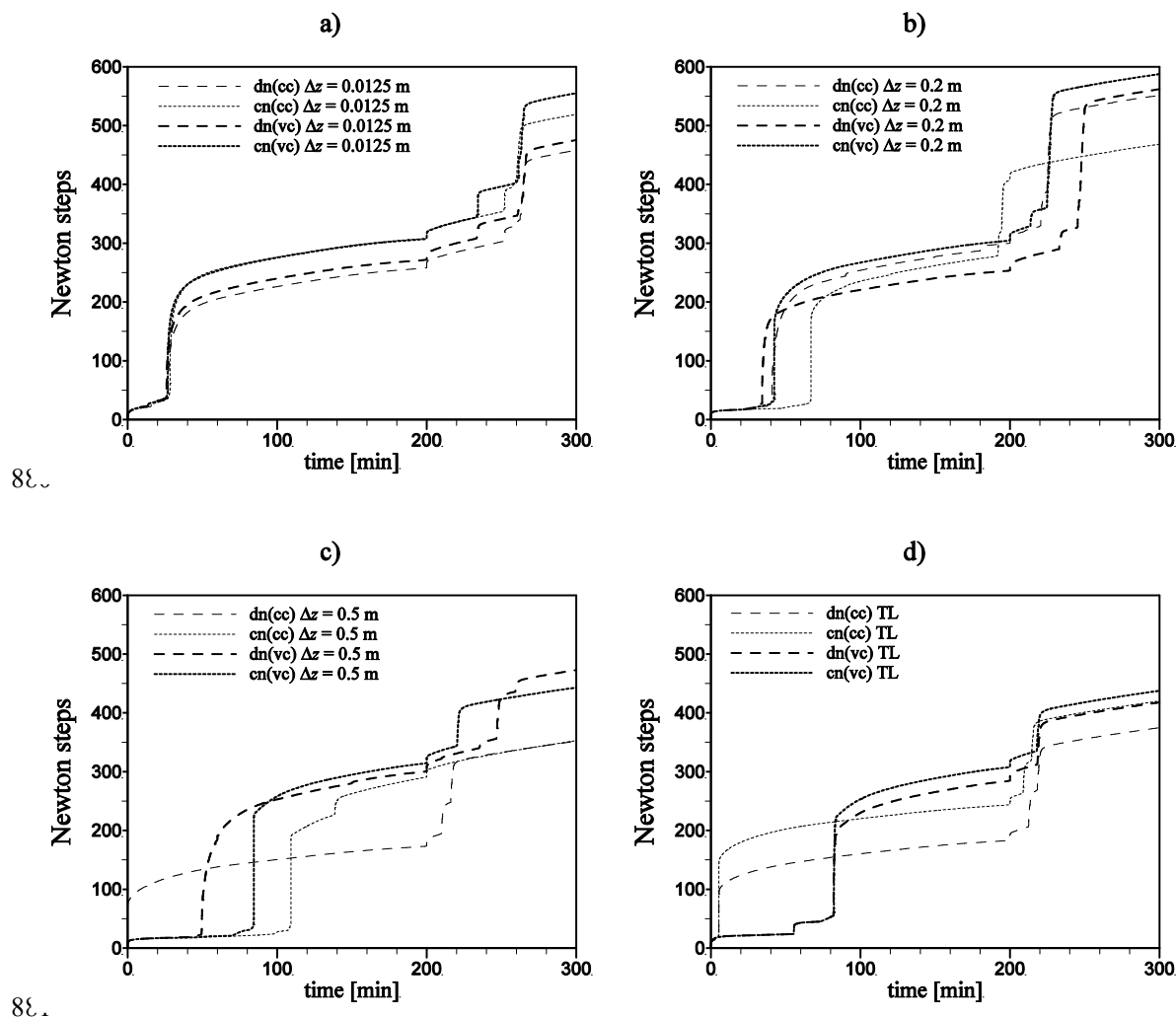
875

876

877

878

879



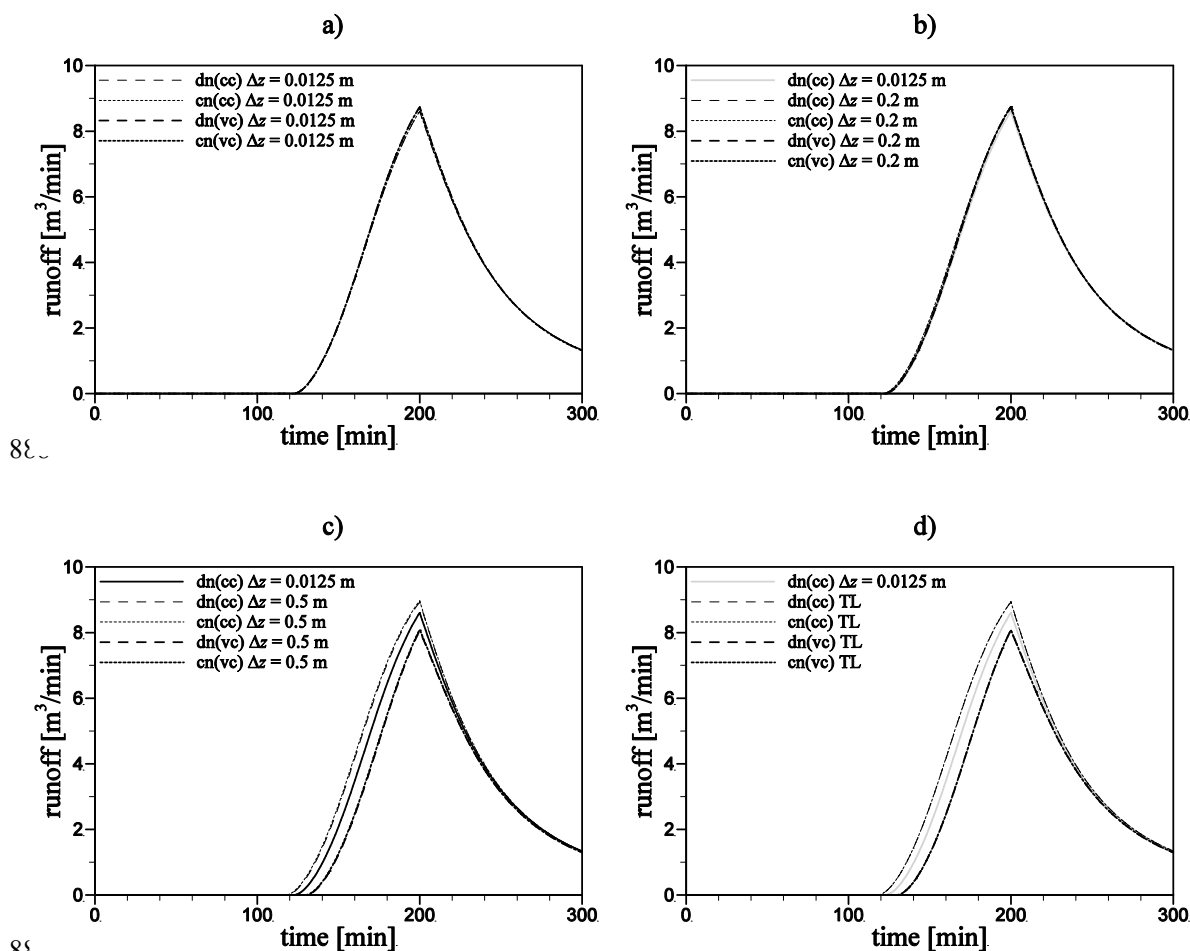
882 Figure 11: The total number of Newton steps for excess infiltration on a hill slope using different vertical
 883 discretizations.

884

885

886

887



890 Figure 12: Outflow response for excess saturation on a hill slope using different vertical discretizations.

891

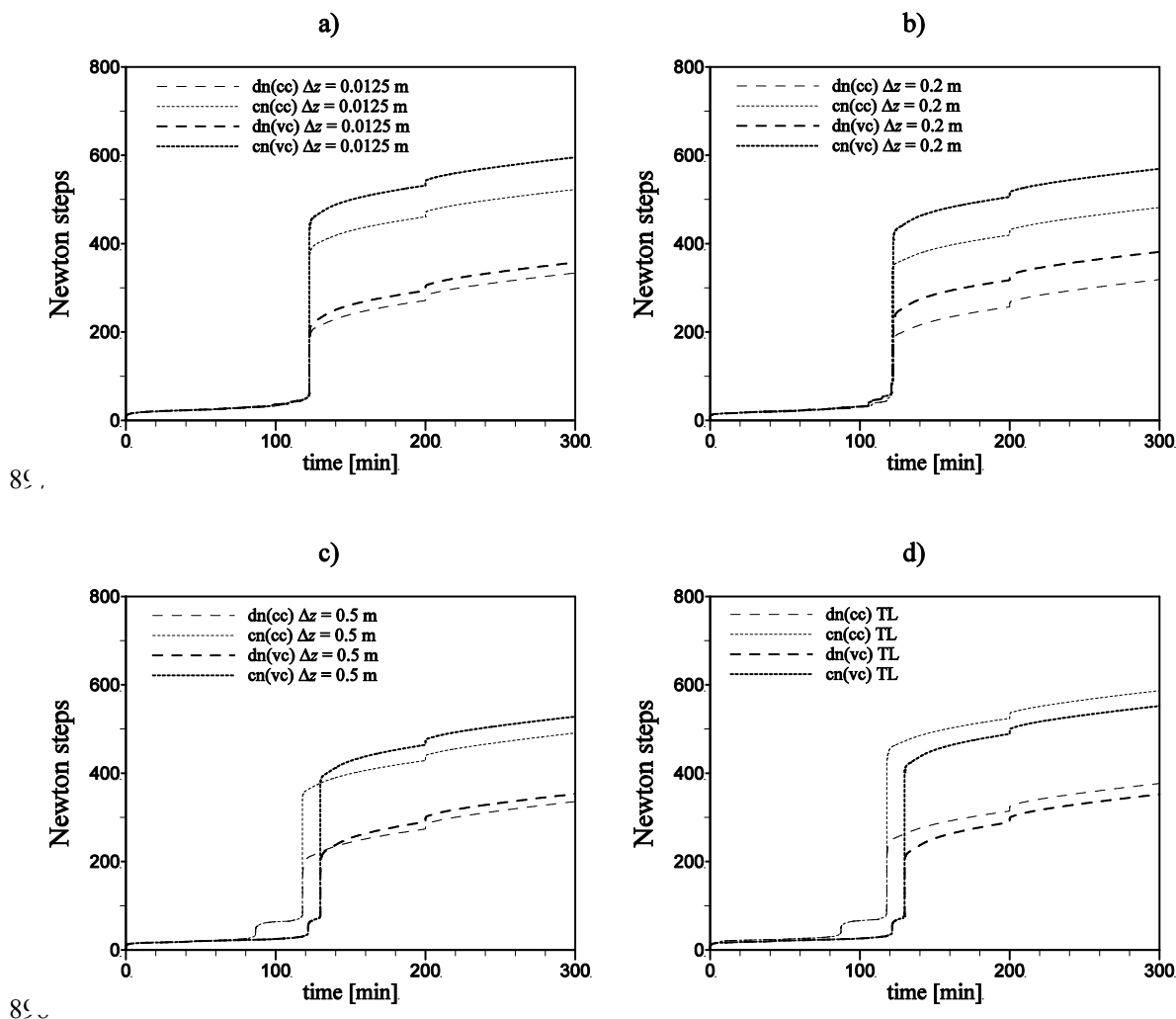
892

893

894

895

896



899 Figure 13: Number of Newton steps for excess saturation on a hill slope using different vertical
 900 discretizations.

901

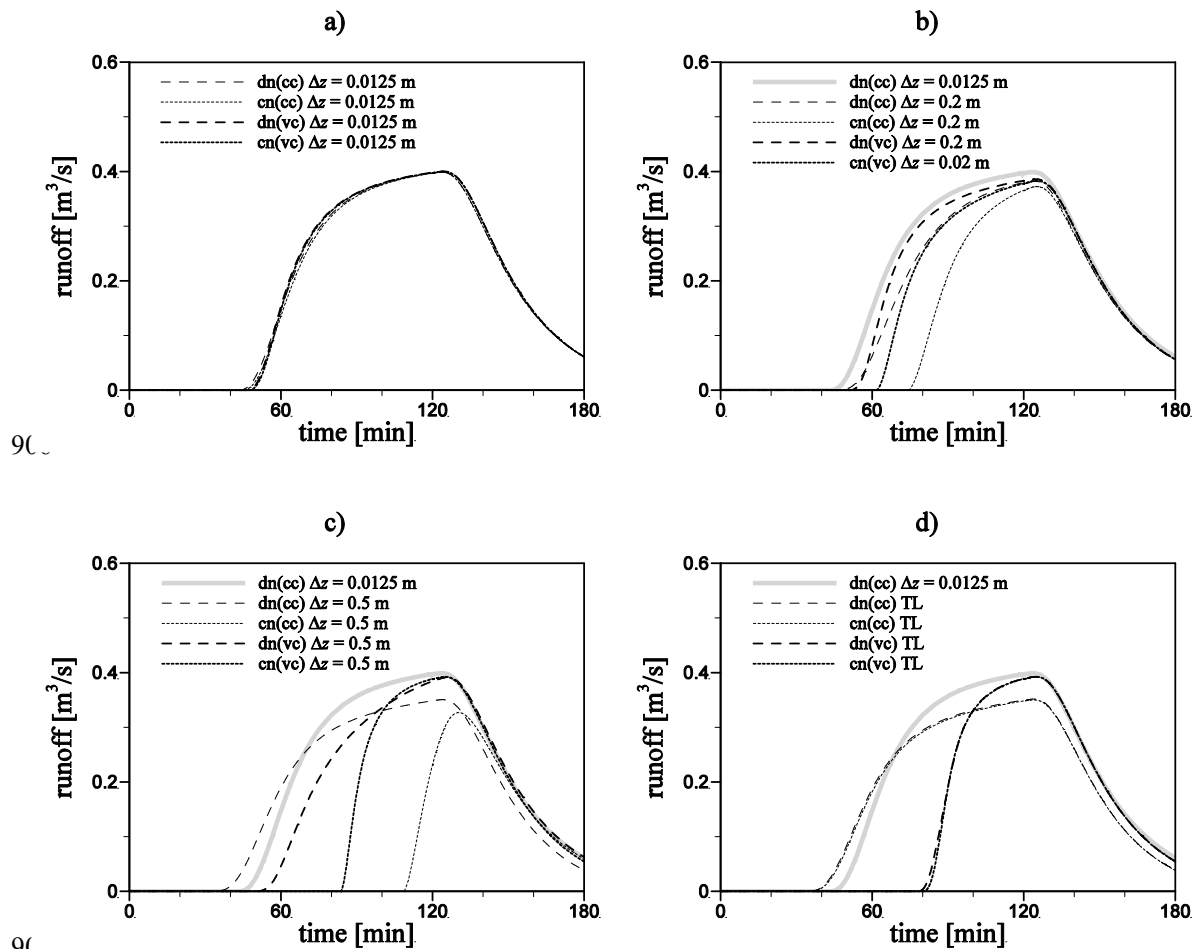
902

903

904



905



906

908 Figure 14: Outflow response for flooding an unsaturated hill slope using different vertical discretizations.

909

910

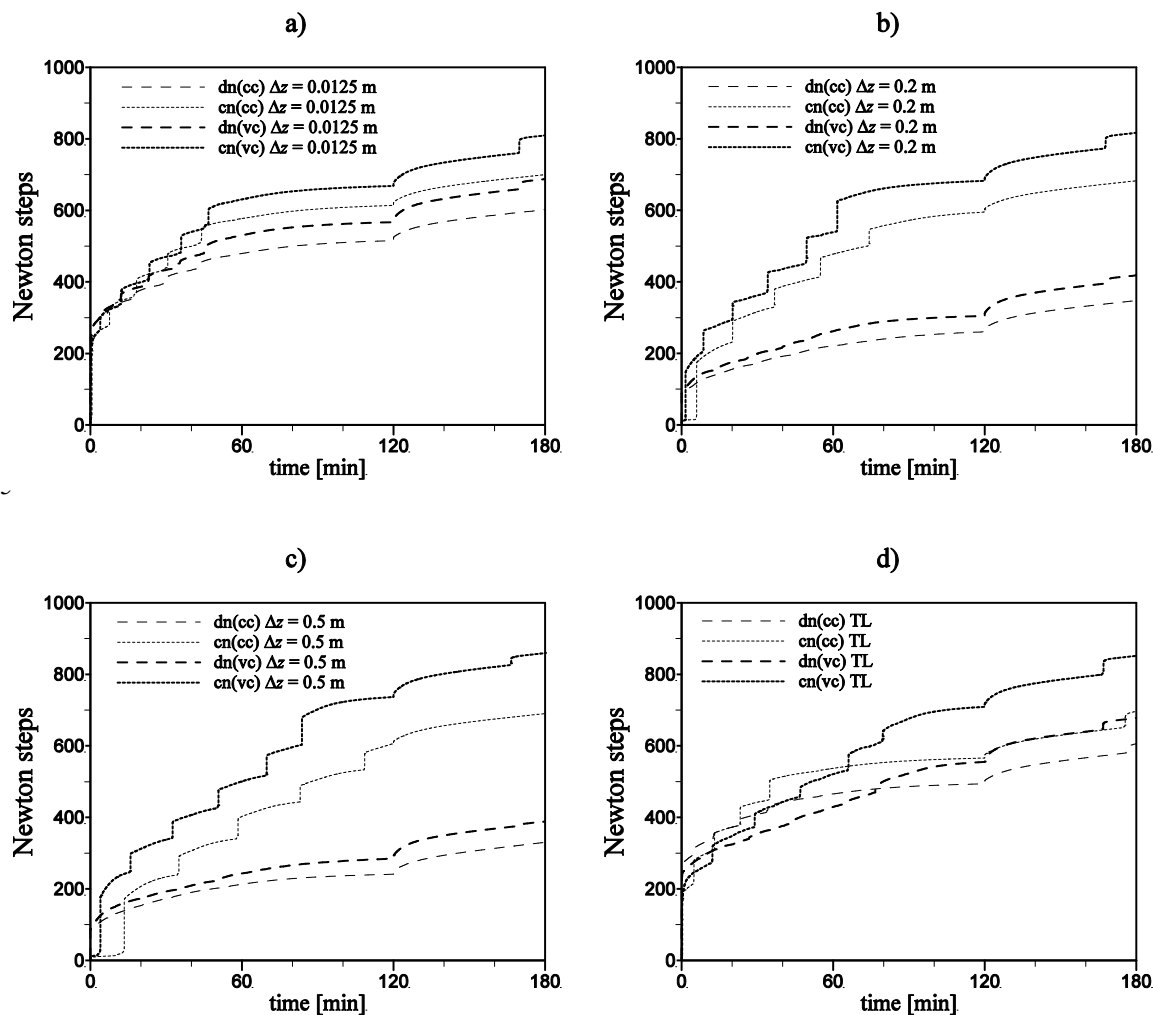
911

912

913



914



915

916

917 Figure 15: Number of Newton steps for flooding an unsaturated hill slope using different vertical
 918 discretizations.

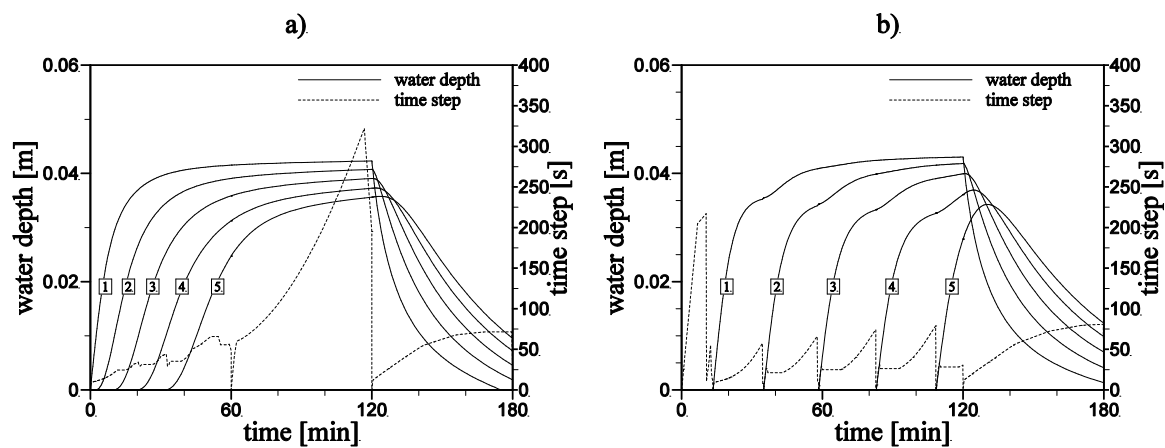
919

920

921



922



923

924 Figure 16: Response in water depth at the five surface nodes (numbered from upstream to downstream) for
925 flooding an unsaturated hill slope. Left: dn(cc) $\Delta z = 0.5$ m. Right: cn(cc) $\Delta z = 0.5$ m.

926

927

928

929

930

931

932

933

934